UNIVERSIDAD DE LAS AMERICAS PUEBLA

School of Sciences

Department of Physics, Actuarial Sciences and Mathematics


# Exclusive Photo-production of $J/\Psi$ and $\Psi(2s)$ as a tool to explore the transition to high and saturated gluon densities at the LHC.

Marco Antonio Alcazar Peredo

164869

Directed by: Dr. Martin Hentschinski

San Andres Cholula, Puebla. Spring-Autumn, 2022

# Contents

# 1. Introduction

By the end of the seventeenth century, J. J. Thomson's idea of corpuscles (now called electrons), deduced from cathode ray experiments [35], made a big leap in the study of the structure of matter because he proposed atoms where divisible and its *corpuscles* were their components. As a result, the plum pudding model was born [36]. In short, this model proposes that the corpuscles with negative charge were distributed inside a big positive charge, just like the raisins are distributed inside a raisin pudding. It was from this discovery that Rutherford's later experiments involving the scattering of alpha particles into a thin metal foil gave rise to more promising descriptions of subatomic structures. Rutherford proposed that the positive charges were not distributed inside a volume but were all concentrated in a single spot. On the other hand, Bohr proposed a model which hinted, with its energy levels at the quantum nature of atoms, and this was eventually refined by other scientists. Electrons continuously leap from one orbital to another and these orbitals had fixed energy levels interchanging light in a discrete spectrum. [11] Thanks to Bohr's model, spectral lines of hydrogen atoms could be predicted. Furthermore, the binding mechanism of protons and neutrons in the atom's core remained unknown.

However, there was still a question not been answered yet. Since protons have a positive charge, it was very contra-intuitive that elements such as boron or aluminium were stable because there is a repelling electromagnetic force between protons inside the nucleus. This would eventually lead scientists to postulate a new force, which in principle, must be stronger than the electromagnetic interaction between the nucleons inside nuclei. Unsurprisingly, came to be known as the *strong nuclear force*. With this new force, many new studies began about the structure of atoms, their components and their interactions.
In order to bind the nucleons, the nuclear force must be approximately 10 million times stronger than the chemical binding that holds atoms together in the forms of molecules [31]. The strong nuclear force has a distinctive characteristic: the range in which is visualized is dramatically short; specifically, one femtometer ($1 \times 10^{-15} m$). Beyond that limit, it decreases

rapidly.

It was until 1935 that Yukawa proposed that nucleons would exchange particles with each other and this mechanism would create the force. [31] This theory was analogous to the electromagnetic force in the sense that a massless particle (the photon) was the cause of the force. Nevertheless, for the nuclear force, Yukawa assumed that the *force-makers* (which were eventually called mesons) carry a mass of a fraction of the nucleon mass. [38] These were called meson theories and later, they were used as models inside a more fundamental theory. Yukawa won the Nobel Price in 1949.

In 1964, the theoretical physicists Gell-Mann and George Zweig [19] proposed something that changed history forever: they proposed each nucleon and each meson is just a bound state of hypothetical particles called *quarks*. According to this theory, these hypothetical particles should exist due to the classification of experimental data and how they interact. These quarks had something very distinct known in the literature as colour charge. In short, the colour charge is an intrinsic property of quarks, antiquarks, and gluons that determine the rules for how these particles interact.

The force between quarks is created when gluons are exchanged between them and is very strong at low energies. [31] Gluons are the particles responsible for holding quarks together in the form of protons and neutrons. Although gluons account for more than 95% of the visible mass of our universe many aspects of these particles are still unknown and their exploration is still a challenge for the contemporary physicist. For example: how do the massless gluons give mass to hadrons (bound states of two or three quarks)? Indeed, if you sum the mass separately from the quarks that conform any hadron, one would realize that this number is not even close to the mass of a complete hadron. Therefore concluding that most of this mass comes from the dynamics of the quarks and gluons.

Another question would be what is the distribution of gluons and quarks inside the proton and the behaviour of systems with high gluon densities at large energies? Or what is the mechanism of confinement due to the fact there are no free colour charges? How do gluons and quarks combine to yield the proton spin?

These overwhelming questions are in the frontier of new physics and are of main concern in

this investigation project.

Particle accelerators presented a radical new way of exploring the microscopic structure of matter. From the first particle accelerator built in Berkeley (Lawrence's Cyclotron) to the most powerful accelerator that humanity has ever built (the Large Hadron Collider), accelerators had permitted us to unravel the insides of hadrons, culminating everything by developing the current best theory to describe the most basic building blocks of the universe: The Standard Model, which explains how these fundamental blocks known as quarks and leptons produce all known matter in the universe.
This model divides particles into two groups according to their spin, fermions (spin 1/2) and bosons (spin 1), where the first group is also divided into quarks and leptons. The standard model states that fermions interactions are due to fields, where the particles associated with them belong to the second group known in the literature as bosons. It also explains how bosons (force-carrying particles) influence quarks and leptons.
An important characteristic of quarks is that they can never be found alone, they are always in groups of two known as mesons or groups of three called baryons. [16].

Now, according to [18], the Deep Inelastic Scattering (DIS) process had its golden age in 1968 thanks to the SLAC-MIT experiment. This experiment gave two interesting results: The first one affirms that the inclusive inelastic cross-section is larger by more than one order of magnitude than expected! Apart from that, it was weakly dependent on the DIS kinematic variable $Q^2$ which is the squared momentum transfer to the lepton. On the other hand, according to [18] at an invariant hadronic mass (W) of the final state larger than 2 $GeV$, the structure-function $F_2$ over a range of $0.7 < Q^2 < 2.3\ GeV$ becomes a function of the ratio $\omega = \nu/Q^2$. These results were very relevant and confirmed the theoretical proposals of physicists like W.K.H. Panovsky, J.D. Bjorken, Dick Taylor and R.P. Feynman.
In short, DIS is a process that occurs in the insides of hadrons using leptons and photons as tools, that aim to explore their insides. Since leptons and photons are fundamental particles, they don't break down into smaller parts and hence they are very useful for this kind of reaction.

Furthermore, this study intends to describe what happens inside hadrons to analyze in more detail a proposal for a new measurement at the Large Hadron Collider (LHC) to detect the possible presence of high densities of gluons. Inside the Large Hadron Collider, apart from the proton-proton collisions in which both protons break up completely, there is a type of reaction that has the characteristic of leaving intact one or both protons when colliding. These kinds of reactions are known as *Ultra Peripheral Collisions*. Even though such events are rare, they are also extremely clean since there is no contamination of the final state due to the proton break-up. Such events have therefore at least in principle the potential to contribute to searches for new physics at the LHC and to cover regions of phase space that are inaccessible to standard searches. The latter process has been already observed at the LHC and can serve as a sort of standard candle to explore this kind of reaction.
The main objective of this research project is the study of the exclusive photo-production of vector mesons at the Large Hadron Collider, and to identify observables that can distinguish between gluon distributions subject to linear and non-linear QCD evolution.

# 2. Quantum Chromodymics

## 2.1 Basic Concepts

### 2.1.1 Hadrons

Ordinary matter is formed by bound states of particles known as *quarks*. The strong nuclear force is responsible for holding them. This force has the property of not sticking all quarks in a single mass, but binding together both quarks and antiquarks into groups of three (qqq or $\overline{qqq}$) or groups of two ($q\overline{q}$).
Consequently, hadrons are divided into three categories:

1. Baryons ($qqq$)
2. Antibaryons ($\overline{qqq}$)

3. Mesons ($q\overline{q}$)

Physicists have great uncertainty while measuring the mass of the quarks. [10] The values proposed in the standard model are approximations of how much a quark could weigh because it is theoretically impossible to isolate one quark. After all, they are bound by the strong interaction. Therefore, it's very difficult to determine how much of the mass of the proton is due to the mass of the quarks versus how much is due to the energy generated by the interaction between the quarks.
All quarks have a baryon number equal to 1/3, and antiquarks have a baryon number equal to $-1/3$.
In addition, quarks have an internal property known as *flavour number*. Each quark has its exclusive flavour number. These values are the following [10]:

- up, charm and top quarks have a flavour number equal to 1
- down, strange, and bottom have a flavour number equal to $-1$

This flavour number is very useful for keeping track of what's happening when diverse quarks interact with each other.
Nonetheless, quarks are the only kind of particle that can experience strong interaction. The feature of the strong force, in contrast with electromagnetic and gravity forces, is that it increments when the distance becomes larger. However, the strong interaction disappears if quarks have separated a distance of $10^{-15}$ m. Quarks can have an opposite particle with opposite *baryon number*. All three quarks have a baryon number equal to 1/3 [10]. In every particle reaction, the total baryon number must be the same before reaction and after the reaction. Something interesting is that the weak force differentiates between quarks and leptons. In other words; it cannot turn a lepton into a quark, and vice-versa.

### 2.1.2 Baryons

Let's consider the first three quarks: up, down and strange.

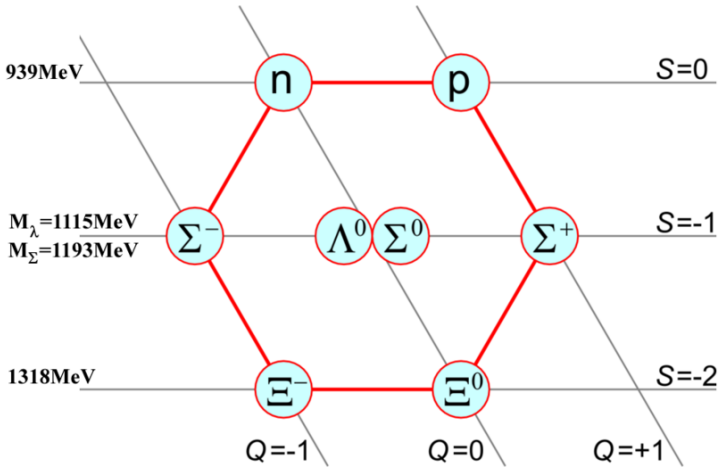


Figure 1: The octet of light spin $-\frac{1}{2}$ baryons described in SU(3). n: neutron, p: proton, $\Lambda$: Lambda baryon, $\Sigma$: Sigma baryon, $\Xi$: Xi baryon. (Venny, 2008)

Horizontal lines are known as baryon families. A family is a set of baryons with similar mass and identical internal properties. The capital S in the first row represents the fact that both particles have the same mass and the same strangeness. And so it continues with the second row: they all have strangeness of -1, and in the third line they all have strangeness of -3. [10]

This diagram is known as the *baryon octet* and it consists of the low-mass quarks combinations. The peculiarity of the octet is that the properties of all the particles are essentially equal, except that some have greater intrinsic energies than others; the greater a baryon's intrinsic energy, the more likely it is to decay.

On the other hand, the uuu, ddd and sss baryons can only exist in higher mass level states.

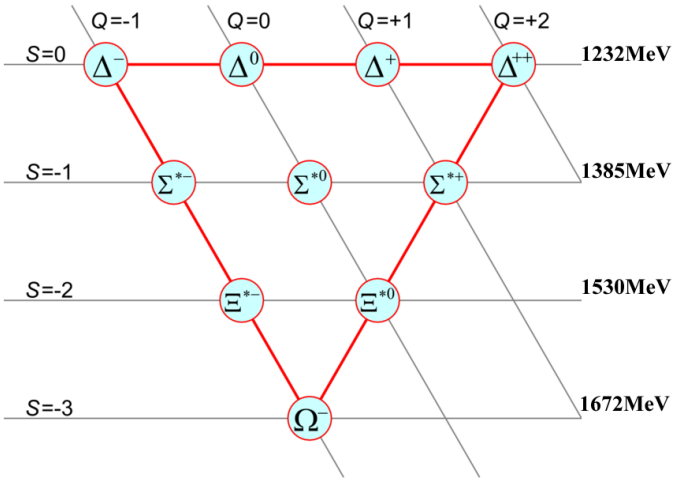


Figure 2: A combination of three up, down or strange quarks with a total spin of $\frac{3}{2}$ form the so-called baryon decuplet. (Venny, 2008)

The above diagram is known as the *baryon decuplet*. It consists of organizing the baryons from a lower mass ($\Delta^+$ is a uud, $\Delta^0$ is a udd or neutron) to a higher mass baryons.
It is worth mentioning that these baryons are formed only by the first three quarks, now if we add the charm quark, the combinations become even more complex. [10]

Finally we can say that the baryons that contain heavy quarks (for example top and bottom quarks) require a tremendous amount of energy to be produced, more than we are capable of providing in laboratories [10].

### 2.1.3 Mesons

For this study, is of special interest to understand what a meson is to understand what a vector meson is. Consequently, this study intends to study the most important definitions of these.

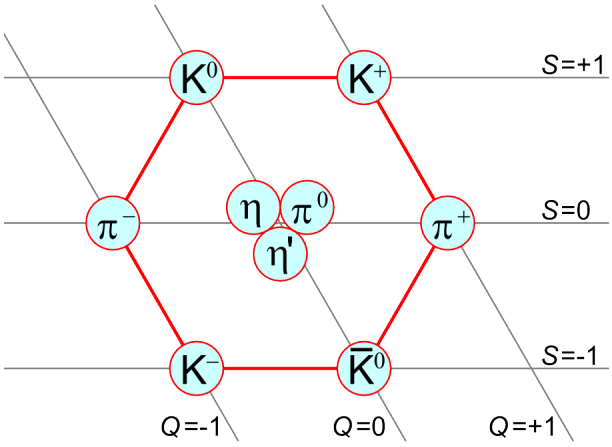


Figure 3: Mesons of spin 0 form a nonet. K: kaon, Π: pion, $\eta$: eta meson. (Public Domain)

As we described before, a meson is a particle formed by a quark and an antiquark. ($q\overline{q}$). It is not a required condition of the meson that the component quark and antiquark be of the same flavour. Any combination is possible, despite the fact some are less plausible. The combinations of light quarks are the most common in nature. As we can see in Figure 3, the strangeness is decreased when we go to the bottom, but the mass doesn't increase. This diagram is known as the meson nonet and the main differences among this family of mesons lie in the way they decay. In a few words, some mesons even have the same mass and electrical charge, yet the way they react when they interact with objects is different. [10]

### 2.1.4 J/Ψ Meson

Is a subatomic particle formed a quark pair (charm-anticharm, $c\,\overline{c}$) which is flavour-neutral, interacts with the four fundamental forces, has spin equal to 1, has a rest mass of 3.096 $\frac{GeV}{c^2}$ and has a mean life-time equal to $7.2 \times 10^{-21}$. [32] Normally, these are mesons created due to a bound state known as *charmonium*, when a quark anti-quark pair is put into a potential. [21] $\Psi(2s)$ is the name the J/Ψ Meson receives when it's in its first excited state. [32] Another relevant fact is that it can decay into a variety of modes; the most relevant ways are:

| | Mode | Fraction ($\Gamma_i/\Gamma$) | Scale factor/ Confidence level |
|---|---|---|---|
| $\Gamma_1$ | hadrons | (87.7 ±0.5 ) % | |
| $\Gamma_2$ | virtual $\gamma \rightarrow$ hadrons | (13.50 ±0.30 ) % | |
| $\Gamma_3$ | $ggg$ | (64.1 ±1.0 ) % | |
| $\Gamma_4$ | $\gamma gg$ | ( 8.8 ±0.5 ) % | |
| $\Gamma_5$ | $e^+e^-$ | ( 5.94 ±0.06 ) % | |
| $\Gamma_6$ | $\mu^+\mu^-$ | ( 5.93 ±0.06 ) % | |

Figure 4: **J/Ψ(1s) Decay Modes**: This figure represents the most plausible decays of the J/Ψ(1s) particle (Nakamura et al., 2010)

### 2.1.5 Scalar and Vector Mesons

There are nine possible combinations of mesons when considering the light quarks, (u, d, s) that can be grouped into an octet and a singlet. [33]. Most of the various hadronic states can be described as states formed by a $q$ and $\overline{q}$ pair. The scalar meson can be defined as a Lorentz group, scalar or pseudo-scalar, which is classified inside the group of particles with irreducible unitary representations of the symmetry group acting on matter fields over space-time. [37] (Wigner Classification) They have even parity and spin 0. Finally, they are the opposite of the vector (or pseudo) mesons and are called vector (or pseudo) representations. As well as the scalar mesons, a vector meson is a meson that is classified inside the group of particles with irreducible unitary representations of the symmetry group acting on matter fields over space-time and is in pseudo-vector or vector representation of the Lorentz Group. What differentiates a vector meson from a scalar meson is that vector mesons have spin 1 and odd parity, while scalar mesons have even parity and spin 0 [37] [33].

## 2.2 Microscopic description in terms of quarks and gluons

### 2.2.1 Lagrangian of QCD

*Quantum Chromodynamics* is the quantum field theory that describes the strong interactions [20], also is defined as the SU(3) gauge theory of the current standard model for elementary particles and forces which encompasses the strong, electromagnetic, and weak interactions. The Feynmann Rules, elegantly, can be derived from the QCD Lagrangian. To obtain the perturbative of any kind of process, we need the Feynmann rules to describe the possible interactions that could happen between gluons and quarks. The Lagrangian density deploys this Feynmann rules, used to describe a perturbative analysis of the QCD theory. The Lagrangian is given by:

$$\mathcal{L}_{classical} + \mathcal{L}_{gauge-fixing} + \mathcal{L}_{ghost} \tag{1}$$

The Lagrangian has to be constructed requiring local gauge invariance under a gauge group $SU(3)_{colour}$. It is worth mentioning that we implement the Einstein sum convention, where the repeated indices are summed over. Making this clear, the expression for the Classical Lagrange Density is according to [17] has the following form:

$$\mathcal{L}_{classical} = -\frac{1}{4}F^{\mathbf{A}}_{\alpha\beta}F^{\mathbf{A}}_{\alpha\beta} + \sum_{flavours} \overline{q}_a(i\not{D} - m)_{ab}q_b \tag{2}$$

These terms are the description of the interaction of a quark with spin $1/2$, with mass $m$ and mass-less gluons with spin $-1$. $\not{D}$ is just the simplified notation for $\gamma_\mu D^\mu$, and the explicit sum runs over the $n_f$ different flavours. We have followed the notation of Bjorken and Drell, with the metric equal to $g^{\alpha\beta} = diag(-1,-1,-1,-1)$ and setting $\overline{h} = c = 1$. The gamma matrices are given by:

$$\gamma^0 = \begin{pmatrix} 1 & 0 & 0 & 0 \\ 0 & 1 & 0 & 0 \\ 0 & 0 & -1 & 0 \\ 0 & 0 & 0 & -1 \end{pmatrix} \tag{3}$$

$$\gamma^1 = \begin{pmatrix} 0 & 0 & 0 & 1 \\ 0 & 0 & 1 & 0 \\ 0 & -1 & 0 & 0 \\ -1 & 0 & 0 & 0 \end{pmatrix} \tag{4}$$

$$\gamma^2 = \begin{pmatrix} 0 & 0 & 0 & -i \\ 0 & 0 & i & 0 \\ 0 & i & 0 & 0 \\ -i & 0 & 0 & 0 \end{pmatrix} \tag{5}$$

$$\gamma^3 = \begin{pmatrix} 0 & 0 & 1 & 0 \\ 0 & 0 & 0 & -1 \\ -1 & 0 & 0 & 0 \\ 0 & 1 & 0 & 0 \end{pmatrix} \tag{6}$$

These matrices satisfy the anticonmmutation relations and take into account the spin of fermions:

$$\gamma^\mu, \gamma^n = 2g^{\mu n}$$

Now, $F^{\mathbf{A}}_{\alpha\beta}$ is the field strenght dericed from the gluon field $A^A_\alpha$:

$$F^{\mathbf{A}}_{\alpha\beta} = [\partial_\alpha \mathbf{A}^{\mathbf{A}}_\beta - \partial_\beta \mathbf{A}^{\mathbf{A}}_\alpha - g f^{ABC} \mathbf{A}^B_\alpha \mathbf{A}^C_\beta] \tag{7}$$

where the indices A, B, and C run over eight different colour degrees of freedom in the gluon field. [17] The third term ($g f^{ABC} \mathbf{A}^B_\alpha \mathbf{A}^C_\beta$) describes the triplet and quartic gluon self-interactions and to the property of asymptotic freedom, similarly, $g$ represents the coupling constant which determines the magnitude of the interaction between coloured quanta and $f^{ABC}(A, B, C = 1, ..., 8)$ are the structure constants of the SU(3) colour group. [17] QCD is a non-Abelian gauge theory which means that the gluon field can interact with itself. At the level of the Lagrangian, this reflects itself in terms of cubic and quadratic terms in the

gluonic field.

Now, the quark fields $q_a$ are the triplet picture of the colour group (a=1,2,3) and D is the covariant derivative goes from [17]:

$$D(\alpha)_{ab} = \partial_\alpha \delta_{ab} + ig(t^C A^C_\alpha)_{ab} \tag{8}$$

to

$$D(\alpha)_{AB} = \partial_\alpha \delta_{AB} + ig(T^C A^C_\alpha)_{ab} \tag{9}$$

where t and T are matrices in the fundamental and adjoint representation of the SU(3) group which satisfy the following commutation relation:

$$[t^A, t^b] = if^{ABC}t^c, \tag{10}$$

and

$$[T^A, T^C] = if^{ABC}T^C \tag{11}$$

The generators in the adjoint representation are related to the structure constants through:

$$(T^A)_{BC} = -if^{ABC} \tag{12}$$

A representation for the generators $t^A$ in the fundamental representation is provided by the eight Gell-Mann matrices, that has the characteristic of being hermitian and traceless. The generators are often written on a standard basis, where $\lambda^a$ represents the Gell-Mann-Matrices: [17]

$$T^a = \frac{1}{2}\lambda^a \tag{13}$$

the coefficient $a$ of $\lambda^a$ runs from 1 to 8 and has the following form:

$$\lambda_1 = \begin{pmatrix} 0 & 1 & 0 \\ 1 & 0 & 0 \\ 0 & 0 & 0 \end{pmatrix}, \ \lambda_2 = \begin{pmatrix} 0 & -i & 0 \\ i & 0 & 0 \\ 0 & 0 & 0 \end{pmatrix}, \ \lambda_3 = \begin{pmatrix} 1 & 0 & 0 \\ 0 & -1 & 0 \\ 0 & 0 & 0 \end{pmatrix}, \ \lambda_4 = \begin{pmatrix} 0 & 0 & 1 \\ 0 & 0 & 0 \\ 1 & 0 & 0 \end{pmatrix} \tag{14}$$

$$\lambda_5 = \begin{pmatrix} 0 & 0 & -i \\ 0 & 0 & 0 \\ i & 0 & 0 \end{pmatrix} , \lambda_6 = \begin{pmatrix} 0 & 0 & 0 \\ 0 & 0 & 1 \\ 0 & 1 & 0 \end{pmatrix} , \lambda_7 = \begin{pmatrix} 0 & 0 & 0 \\ 0 & 0 & -i \\ 0 & i & 0 \end{pmatrix} , \lambda_8 = \frac{1}{\sqrt{3}} \begin{pmatrix} 1 & 0 & 0 \\ 0 & 1 & 0 \\ 0 & 0 & -2 \end{pmatrix} \tag{15}$$

By convention, the normalization of the SU(N) matrices is given by: [17]

$$Trt^A t^B = T_R \delta^{AB}, T_R = \frac{1}{2}$$

# 3. Exploring QCD

## 3.1 Deep Inelastic Scattering

In short, Deep Inelastic Scattering (DIS) is a process that occurs in the insides of hadrons using leptons and photons as tools, that aim to explore their insides as if one was using a microscope. [26]

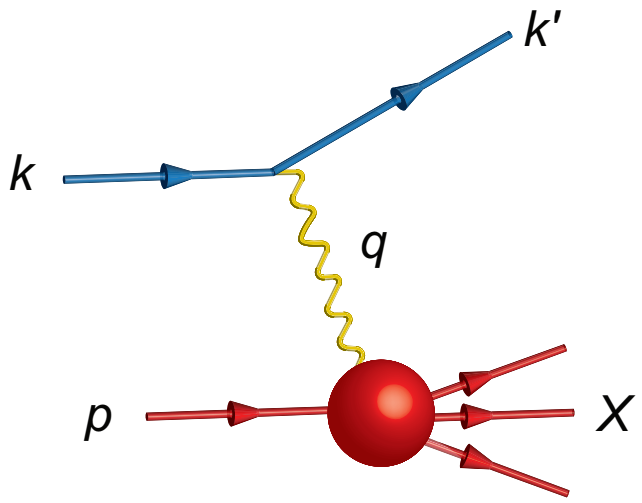


Figure 5: Deep Inelastic Scattering visualization

The kinematic variables for Deep Inelastic Scattering are given by the following:

- $p$ : The four-momentum of a nucleon.
- $k, k'$: The four momenta of the incoming and outgoing lepton
- $\sqrt{s}$: Squared collision energy because of the reaction of the electron and the hadron

$$s = (p + k)^2$$

- $Q^2$: Squared momentum transfer to the lepton, equal to the virtuality of the exchanged photon.

$$Q^2 = -q^2 = -(k - k')^2$$

- $Q$: Resolution of the insides of the hadrons $1/\lambda$
- $x_B$: Bjorken variable which determines the momentum fraction of the parton on which the proton scatters.

$$x = \frac{Q^2}{(W^2 + Q^2)} = \frac{Q^2}{2pq}$$

- $W^2$: The squared invariant mass of the produced hadronic system X.

$$W^2 = (p + q)^2$$

For physical explanation, consider a high-energy scattering in which there is a charged lepton off the hadron target, where the incoming and outgoing lepton four-momenta are $k^\mu$ and $k'^\mu$, a momentum of the hadron target is denoted as $p^\mu$ and the transfer of the momentum is given by the expression $q^\mu = k^\mu - k'^\mu$. The standard DIS is going to be defined as follows: [17]

$$\begin{aligned} Q^2 &= -q^2 \\ M^2 &= p^2 \\ \nu &= pq = M(E' - E) \\ x &= \frac{Q^2}{2v} = \frac{Q^2}{2M(E - E')} \\ y &= \frac{qp}{kp} = 1 - \frac{E'}{E}, \end{aligned}$$

Here the energies are referencing the rest frame of the target, and the variable $M$ is the proton mass.

Continuing with this topic, let us introduce the parametrization of the target which is called Structure Function, $F_i(x, Q_1)$ which is visualized by a virtual photon that is defined in the terms of lepton-scattering cross sections.

Mathematically, this type of scattering will be $lp \to lX$ is given as the following:

$$\frac{d^2\sigma^{em}}{dxdy} = \frac{8\pi\alpha^2 ME}{Q^4}\left[\left(\frac{1+(1-y)^2}{2}\right)2xF_1^{em} + (1-y)(F_2^{em} - 2xF_1^{em}) - (M/2E)xyF_2^{em}\right].$$

Also, there is another particular example of the antineutrino scattering being $\nu p \to lX$:

$$\frac{d^2\sigma^{2\nu(\bar{\nu})}}{dxdy} = \frac{G_F^2 ME}{\pi}\left[(1-y-\frac{M}{2E}xy)F_2^{\nu(\bar{\nu})} + y^2xF_1^{\nu(\bar{\nu})} + y^2xF_1^{\nu(\bar{\nu})} + (-)y(1-1/2y)xF_3^{\nu(\bar{\nu})}\right].$$

In this part of the project is necessary to study a concept known as *Bjorken limit*. When its range is defined as $Q^2$, $\nu \to \infty$ where $x$ is fixed and applying this limit one can observe that it must obey the scaling law:

$$F_i(x, Q^2) \to F_i(x). \tag{16}$$

The Bjorken scaling declares that the virtual photon will scatter as pointlike parts and because the limit is to infinity the usage of the parton model can be transformed into an infinite momentum frame where one will see the proton moving extremely fast $p^\mu(P, 0, 0, P)$ with $P >> M$. Then, employing this model the proton will scatter as a quark that is moving in parallel with the proton and carrying just a fraction of the momentum $\xi$ and the equation is the following one:

$$\frac{d^2\sigma}{dxdQ^2} = \frac{4\pi\alpha^2}{Q^4}\left[[1+(1-y)^2]F_1 + \frac{(1-y)}{x}(F_2 - 2xF_1)\right]. \tag{17}$$

Because these are scatterings they have amplitudes which are related by crossing symmetry that requires the amplitude of a particle momentum $k$ in the initial state to be equal to the

antiparticle with momentum $-k$. This process is the next one:

$$e^-(k) + q(p_q) \to e^-(k') + q(p'_q) \tag{18}$$

$$e^+(-k) + e^-(k) \to \bar{q}^-(-p_q) + q(p'_q) \tag{19}$$

. Applying the Mandelstam variables $\hat{s} = (k + p_q)^2, \hat{t} = (k - k')^2$ and $\hat{u} = (p_q - k')^2$, so the matrix for the amplitude will be this:

$$\bar{\Sigma} = |\mathcal{M}|^2 = 2e_q^2 e^4 \frac{\hat{s}^2 + \hat{u}^2}{\hat{t}^2}. \tag{20}$$

The sum is referring to the average colours and spins. Next, the Mandelstam variables suffer a change in their notation for DIS: $\hat{t} = -Q^2, \hat{u} = \hat{s}(y - 1)$ and $\hat{s} = \xi Q^2/xy$. The result of this for a cross-section of massless $2 \to 2$ scattering will be:

$$\frac{d\hat{\sigma}}{d\hat{t}} = \frac{1}{16\pi\hat{s}^2}\bar{\Sigma} = |\mathcal{M}|^2, \tag{21}$$

and doing a substitution in the matrix the expression is simplified as follows:

$$\frac{d\hat{q}}{dQ^2} = \frac{2\pi\alpha^2 e_q^2}{Q^4}[1 + (1 - y)^2]. \tag{22}$$

Another important equation is the mass-shell constraint for the outgoing quark:

$$p_q'^{\,2} = (p_q + q)^2 = q^2 + 2p_q q = -2pq(x - \xi) = 0. \tag{23}$$

With the previous equations and writing $\int_0^1 dx\delta(x - \xi) = 1$, the result is the double differential cross section for the quark scattering process defined as:

$$\frac{d^2\hat{\sigma}}{dxdQ^2} = \frac{4\pi\alpha^2}{Q^4}[1 + (1 - y)^2]\frac{1}{2}e_q^2\delta(x - \xi). \tag{24}$$

Having all these equations and concepts we can observe that the structure functions are:

$$\hat{F}_2 = xe_q^2\delta(x - \xi) = 2x\hat{F}_1. \tag{25}$$

So, this equation proves that a quark is a constituent with a momentum fraction $\xi = x$. This gives origin to a set of observations of the naive parton model:

- $q(\xi)d\xi$ represents the probability of a quark having momentum in the range of $\xi$ and $\xi + d\xi$, where $0 \leq \xi \leq 1$.
- Virtual photon scatters incoherently off the quark constituents [26].

The probability distribution with the weight of the quark structure functions results in the proton structure functions:

$$F_2(x) = 2xF_1 = \sum_{q,\bar{q}} \int_0^1 d\xi q(\xi) x e_q^2 \delta(x - \xi) = \sum_{q,\bar{q}} e_q^2 x q(x). \tag{26}$$

A particular case is the scattering of a charged lepton off a proton target originated by a virtual photon exchange that has four quark flavours:

$$F_2^{em}(x) = x[4/9(u(x) + \bar{u}(x) + c(x) + \bar{c}(x)) + 1/9(d(x) + \bar{d}(x) + s(x) + \bar{s}(x))]. \tag{27}$$

In the specific case of the neutrino scattering with $\nu p \to lX$, the virtual $W^+$ gives the measures of the quark distribution weighted by a weak charge:

$$F_2^{\nu}(x) = 2x[d(x) + s(x) + \bar{u}(x) + \bar{c}(x)]. \tag{28}$$

## 3.2 HERA as a tool to explore DIS

HERA was the largest particle accelerator at DESY and Germany's largest research instrument. [24] For 15 years, the storage ring was useful for the international particle physics community because it's the world's most precise electron microscope for studies of the proton's inner structure. Despite the fact the HERA experiments H1, ZEUS and HERMES were shut down in 2007, the ongoing data analysis continues to point the way for future particle physics experiments. The only facility in the world where two different types of particles were first accelerated separately and then brought to the collision was at DESY, in The HERA storage ring. Deep below Hamburg, lightweight electrons or positrons collided with hydrogen nuclei like protons, which are 2000 times heavier, in a 6.3-kilometre-long tunnel. [24] The point-like electrons in these collisions act like slight examination, revealing the inner structure of the proton by scanning its inside. Physicists gaze deeper into a proton

and obtain more of its inner structure insights and fundamental forces of nature when the energy of the particle collision is higher. Large international teams of researchers operated four immense detectors at the HERA storage ring. In 1992 the H1 and ZEUS experiments went into operation. To unravel the inner structure of the proton and the mysteries of the essential forces, they inspected the high-energy collisions of electrons and protons. In 1995 the HERMES experiment began to take data by using the HERA electron beam to inspect the peculiar angular momentum of protons and neutrons, the spin. The HERA-B experiment used the HERA proton beam from 1999 to 2003, to shed light on the properties of heavy quarks. Until 2007, the H1, ZEUS, and HERMES were in operation recording a massive amount of data. During this period, a countless amount of insights that HERA provided into microcosm became a part of physics textbooks. [24] They turned into a basic part of the knowledge we have of the working of our world. However, the outing of discovery is far from over. Astonishing insights into the inner structure of the proton and essential forces of nature for years to come will be implemented by the evaluation of the recorded measurement data. H1 and ZEUS discovered that the proton contains a seething particle soup in which quarks, antiquarks and the gluons that constantly act between them appear and disappear invariably. Also, H1 and ZEUS were able to provide direct evidence with the electromagnetic and weak forces, two essential forces, that have the same origin: the electroweak force, into which the two forces unite at extremely high energies. The HERA experiments in this manner directly examined the effects of the first step toward the grand unification of the four essential forces of nature. H1 and ZEUS have also precisely measured the strong force that acts between quarks. For the first time, over a wide range of energies, consistently demonstrated that the strength of this force changes in the opposite manner from the other forces of nature: Quarks move more freely the closer they are to one another. The farther they are apart, the stronger the pull of the strong force that draws them back together. [24] To have a more deeply understanding of the spin of the protons and neutrons, researchers must analyze the contribution each member of the seething particle soup inside them makes. This was the strength of HERMES. The experimentâs special concept enabled physicists to measure the contribution made by each different type of quark to the total spin, separately. In addition, HERMES was among the first experiments in the world to convey

direct evidence of gluon spin. [24]

## 3.3 QCD at small x

### 3.3.1 Non-linear Evolution

The simplest model of a proton can be explained through the interaction of 3 quarks (two up quarks and one down quark) employing gluons exchange, this has been corroborated by experiments done by HERA (Hadron-Electron Ring Accelerator), RHIC (The Relativistic Heavy Ion Collider) and LHC (The Large Hadron Collider) colliders. [5]

In high-energy scattering experiments, we encounter fluctuations in the form of quarks, anti-quarks, and diverse gluons, popping in and out of existence. When we accelerate a proton near the speed of light, due to the Lorentz time dilation, the gluons that engender from quantum fluctuation have a longer lifetime. By speeding the proton up, the gluon fluctuations slow down sufficiently to take "snapshots" of them with a probe particle, which was sent to interact with the proton.

Probing the proton wave function is done by the interaction using a lepton, they exchange a (virtually) photon. The photon's virtuality ($Q^2$), determines the size of the transverse plane region to the ray axis probed by the photon, with a width of $\Delta r_T \sim 1/Q$. The *Bjorken* $x$ is the fraction of the proton momentum carried by the struck quark. At high energies, $x^2/W^2$ where $W$ is the centre of mass energy of the photon-proton system, at last, small values of $x$ indicate high-energy scattering. [5]
The PDFs of the "sea" gluons $G$ and "sea" quarks $xS$ increase when taking into account a low $x$ (which are scaled down to fit the figure). Here the gluon distribution is more dominated as we reach $x < 0.1$, determining, at high energies (low $x$) the part of the wave-function accountable for the high energies interactions are overall of gluons. [5]
The small-$x$ wave function is dominated by gluons. This dense regime most commonly uses QCD evolution equations. These evolution equations allow us to determine the distributions

at values $(x, Q^2)$ if they are firstly known at other values $((x_0, Q_0^2)$. When first indicating the value of $Q_0^2$ the equation Dokshitzer-GribovLipatov-Altarelli-Parisi (DGLAP) permits us to establish the parton distribution at $Q^2 > Q_0^2$ at all $x$ where the DGLAP is actionable. For low-$x$ for values $x_0 > x$ and all $Q^2$ to assemble the parton distributions the Balitsky-Fadin-Kuraev-Lipatov (BFKL) evolution equation is used. The emerging question is if the quark or the gluon densities can increase without limit at small-$x$. In QCD there is not a tight limit on the density of gluons, but there is a limit in the scattering cross-sections. A proton with multiple "sea" gluons has more affinity to interact in high energy scattering which creates a larger cross-section. The bound on cross-sections $\omega_{tot} \leq 2\pi R^2$ (which comes from the black disk limit in quantum mechanics) have repercussions in the density of gluons. [5]

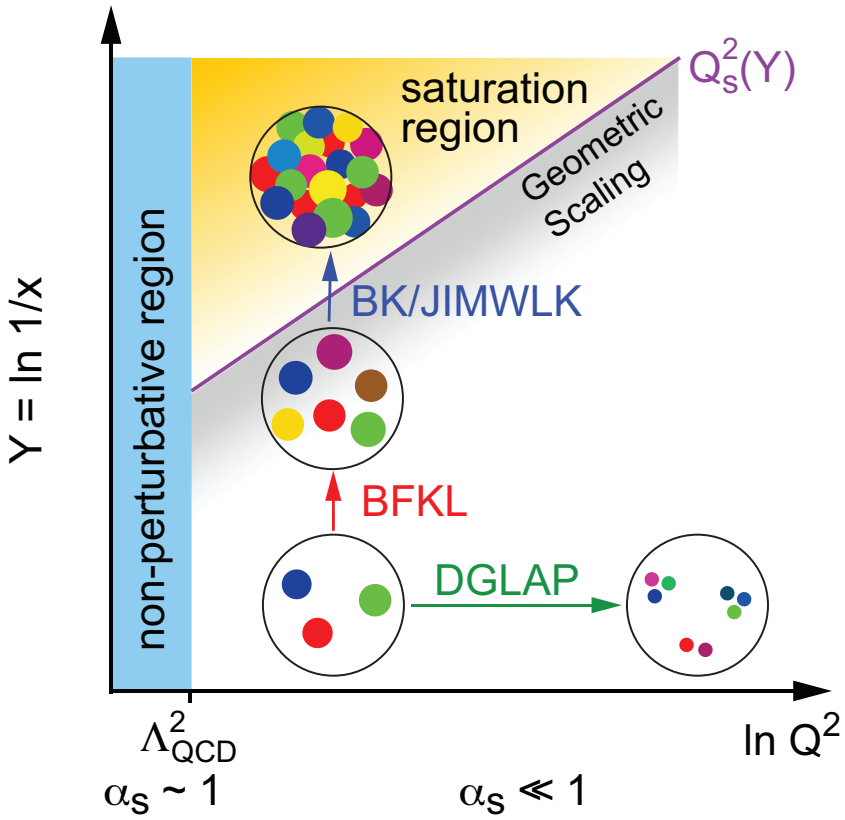


Figure 6: The map of high energy QCD in the $(Q^2, Y = \ln 1/x)$ plane. [5]

# 4. Photo-production of Vector mesons $J/\Psi$ and $\Psi(2s)$ in ultaperipheral collisions at the LHC

## 4.1 The LHC as a tool to explore low x QCD

Alike the HERA experiment, the Large Hadron Collider (LHC) is a two-ring superconducting hadron accelerator and collider installed in the existing 26.7 km tunnel geometry, that was originally designed for the electron-positron machine (LEP), and was constructed between 1984 and 1989 [1]. Since the LHC's main aim is to reveal the physics beyond and inside the Standard Model with a centre of mass collision energies up to $\sqrt{s} = 14$ TeV, it's perfect for exploring low x QCD due to its high centre of mass energy. It collides 2 beams of either protons or ions at colossal speeds (closer to the speed of light) allowing scientists to reproduce the conditions that existed within a billionth of a second after the Big Bang. [1] It, therefore, allows to investigate questions related to the behaviour of perturbative Quantum Chromodynamics at the highest centre of mass energies; in particular, questions related to the possible transitions in a regime, where QCD evolution turns non-linear, characterized by the presence of high gluon densities. Finally, it is worth mentioning that the quarks are the most fundamental blocks that build all the matter in our universe (hadronic matter). Thereupon, thanks to LHC we gain a better understanding of how are the interactions, decay, and intrinsic properties of the standard model. [1] It had found new bound states of exotic particles, CP-violating decays, and neutral current conservation, in other words: Everything it has ever seen in the collider is in 100% agreement with the Standard Model. Therefore, all of this data extracted from both the LHC and HERA is fundamental for this study due to the fact theoretical predictions for the saturation and distributions of gluons inside the nuclei will be made. All these theoretical predictions will be compared and fitted to this experimental data so we can verify the energy dependency of the photo-production cross-section and intend to describe the gluon distributions inside the nuclei.

The detectors from the LHC that will be used are The Large Hadron Collider beauty (LHCb)

experiment, which is specialized in investigating the subtle differences between matter and antimatter employing one type of particle called the beauty or bottom quark. [1]. On the other hand, data taken from ALICE (A Large Ion Collider Experiment) will also be used. The main purpose of this detector is to study the heavy-ion physics at the Large Hadron Collider (LHC). [1] It also studies the matter interacting within the strong nuclear force at extreme energy densities, where a phase of matter called quark-gluon plasma forms, likewise H1 and ALICE experiments.

## 4.2 Ultra-Peripheral Collisions

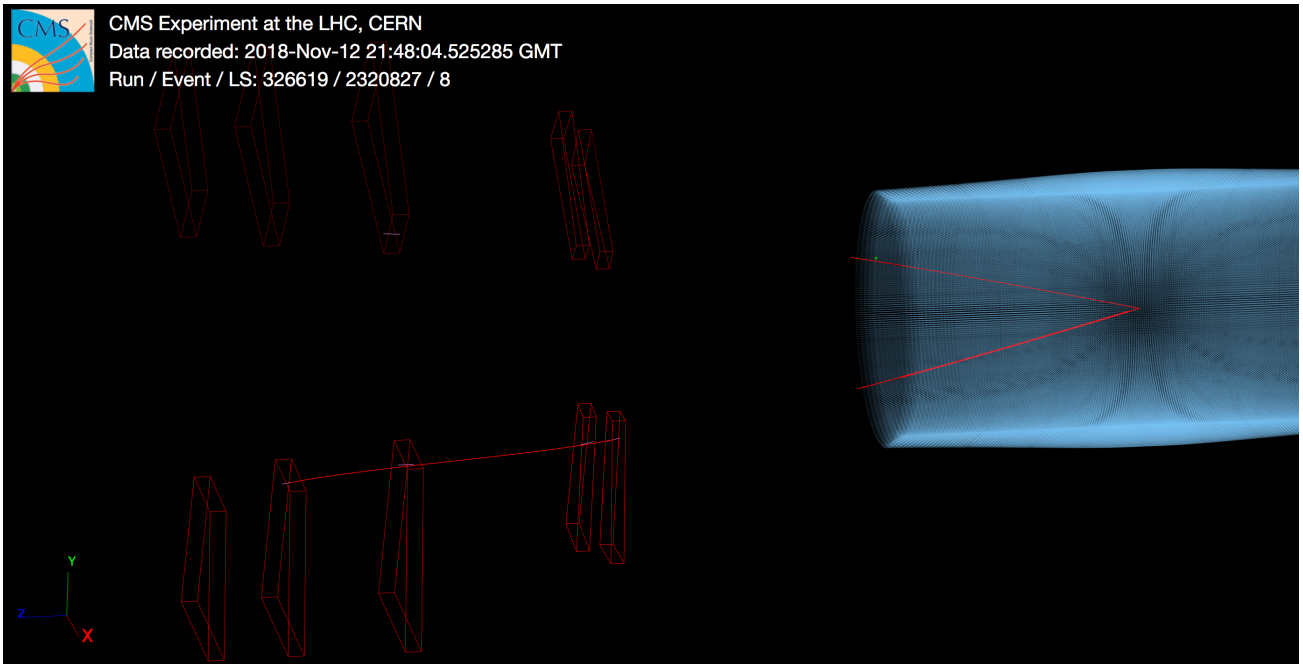


Figure 7: An event where a candidate $J/\Psi$ is produced in an ultra-peripheral Pb-Pb collision and decays to two muons that are represented as red lines within the blue cylinder. (Cauley and Thomas CMS Collaboration, 2018)

An important physical phenomenon that occurs when two nuclei collide can be the following:

- A photon originated from one ion striking another one or

- A certain number of photons coming from each nucleus colliding with each other is called a photon-photon collision.

There is still one more event: **Ultra-peripheral hadron-hadron collisions** (UPS's). This kind of collision occurs in the LHC and its process consists of proton-proton taking place in the centre of the mass energies that have a magnitude of higher order with some photon-heavy ion collisions reaching almost 30 times the energies available in certain target accelerators.

These processes are of the electromagnetic kind and their fields of heavy ions tend to be strong and have multi-photon reactions. Another Ultra-relativistic heavy ion interactions are used to study nuclear photon excitation and photoproduction of hadrons and generate strong electromagnetic fields from a heavy ion and permit some multi-photon excitation of nuclear targets [27]. The result of these collisions is the high-level energy states in the nuclei an event called double-giant resonance, as seen in figure 7.

Entering in some mathematical formalism and a physical concept one must introduce the cross section for photoproduction of a state $x$ given as follows:

$$\sigma_X = \int d\omega \frac{n(\omega)}{\omega} \sigma_X^{\gamma}(\omega), \tag{29}$$

where $\sigma_X^{\gamma}(\omega)$ is the photonuclear cross section [27]. A special case is the one in the highest energy colliders the reactions $\gamma\gamma \to X$ that help to probe the contents of the quark and its spin structure of the meson resonances. Another physical event is the production of mesons that support the internal structure of hadrons in the LHC and they detect electroweak processes $\gamma\gamma \to W^+W^-$.

Mathematically, the cross-section for two-photon processes is given by the next expression:

$$\sigma_X = \int d\omega_1 d\omega_2 \frac{n(\omega_1)}{\omega_1} \frac{n(\omega_2)}{\omega_2} \sigma_X^{\gamma\gamma}(\omega_1, \omega_2), \tag{30}$$

where $\sigma_X^{\gamma\gamma}(\omega_1, \omega_2)$ refers to the homonym concept.

The peripheral collisions have a relation with Fermi's method because it permits the work

with strong interactions and the nuclei. Also, the advance in the relativistic of heavy-ion accelerated it is thanks to this method.

### 4.2.1 Photon Flux

The present concept refers to the flux of a group of photons originated from a charged particle given by applying the Fourier transform to an electromagnetic field of a certain moving charge.

In figure 8, observe that fields stated in the relativistic particle of Lorentz are contracting the pancake and the resultant statement is that the spectrum of the photon energy is dependable on the time target particle maintains inside the pancake and the minimum photon wavelength is equivalent to the width of pancake at the target [27].

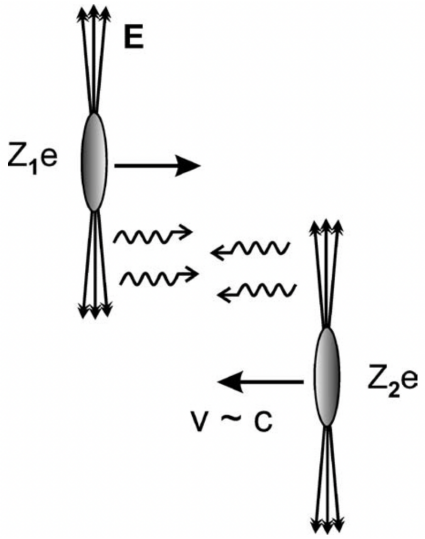


Figure 8: Model of the high electrical charges that are contracted by electric fields.

One can also have the maximum photon energy calculated as follows:

$$\omega^{max} = \frac{\hbar}{\Delta t} \sim \frac{\gamma \hbar v}{b}. \tag{31}$$

The $\gamma$ factor is Lorentz relation where $\gamma = (1 - v^2/c^2)^{-1/2}$. To understand this better, create a target frame applying the previous equation with the restriction in $\gamma$ which has to

be taken just as the boost moves from one frame to another ($\gamma = 2\gamma^2_{collider} - 1$) [27]. Now, for the experimental aspect of the ultra-peripheral collisions (UPC) have a list of interesting features such as final state multiplicity being smaller with events that are fully reconstructed. The reason for the last characteristic is that the interactions between photons are small in a two-photon interaction, so the final state is smaller as well. The adaptation of UPC is applied in the accelerators of different classes. The most important accelerator is the LHC which is testing a UPC program that includes a great list of experiments specifically about *pp* collisions and the usage of ion beams that gives lower photon energies.

## 4.3 Wave-functions

### 4.3.1 Light-Cone quarkonia wave function

According to [12] the light-cone quarkonium wave function for the $J/\Psi$ vector meson is denoted as $\Psi_V(r, z)$ and it's defined in the infinite momentum frame such as the light-cone photon-quark wave function $\Psi^{T,L}_{\gamma^*}(r, z; Q^2)$.

In the $q\bar{q}$ rest frame, the quarkonia wave function is usually found by solving the following Schrödinger equation for a given choice of the heavy quark interaction potential: [12]

$$\left(-\frac{\Delta}{2\mu}\right)\Psi_{nlm}(\tilde{r})\Psi_{nlm}\vec{\tilde{r}} = E_{nl}\Psi nlm\vec{\tilde{r}} \tag{32}$$

with

$$\mu = \frac{m_Q}{2}$$

where $\mu$ is the reduced mass of the $q\bar{q}$ pair and the operator $\Delta$ acts on the coordinate $\tilde{r}$ as follows:

$$\Delta = \sum_{i=1}^{3}\frac{\partial^2}{\partial x_i^2} = \frac{1}{\tilde{r}^2}\frac{\partial}{\partial\tilde{r}}\left(\tilde{r}^2\frac{\partial}{\partial\tilde{r}}\right) + \frac{1}{\tilde{r}^2\sin\theta}\frac{\partial}{\partial\theta}\left(\sin\theta\frac{\partial}{\partial\theta}\right) + \frac{1}{\tilde{r}^2\sin^2\theta}\frac{\partial^2}{\partial\phi^2} \tag{33}$$

Now, factorizing the spatial wave function into the radial and angular parts:

$$\Psi_{nlm}\vec{\tilde{r}}Y_{lm}(\theta, \psi) \tag{34}$$

using equations (32) and (34) the Schrödinger equation as the following two equations:

$$\frac{1}{\tilde{r}}\frac{\partial^2}{\partial\tilde{r}^2}\left(\tilde{r}\Psi(\tilde{r}) + m_Q(E - V(\tilde{r}))\,\Psi(\tilde{r}\right) = \frac{l(l+1)}{\tilde{r}^2}\Psi(\tilde{r}) \tag{35}$$

and

$$\frac{1}{\sin\theta}\frac{\partial}{\partial\theta}\left(\sin\theta\frac{\partial Y(\theta,\phi)}{\partial\theta}\right) + \frac{1}{\sin^2\theta}\frac{\partial^2 Y(\theta,\phi)}{\partial\phi^2} = -l(l+1)Y(\theta,\phi) \tag{36}$$

Now, it is needed to define the quarkonia wave functions for the radially excited vector meson $\Psi(2s)$. As in the $J/\Psi$ quarkonia wave function, these functions are defined in the $q\bar{q}$ rest frame. It is obtained by solving the following Schrödinger equation for a given potential: [29]

$$\left(\frac{\Delta_r}{m_Q} + V_{Q\bar{Q}}(r)\right)\Psi_{nlm}(\vec{r}) = E_{nl}\Psi_{nlm}(\vec{r}) \tag{37}$$

where the wave function $\Psi_{nlm}(\vec{r})$ depends on the three dimensional $q\bar{q}$ separation $\vec{r}$ and factorized has the following form:

$$\Psi_{nlm}(\vec{r}) = \Psi_{nl}(r)\cdot Y_{lm}(\theta,\phi) \tag{38}$$

where $\Psi_{nl}(r)$ denotes the radial part of the wave function and $Y_{lm}(\theta,\phi)$ denotes the orbital part of the same wave function. [29]

We stated that for solving equations (32) and (37) is needed a choice for a heavy quark interaction. For this study, two potentials were implemented: the **Harmonic Oscillator Potential** and the **Buchmüller-Tye Potential**. The Harmonic Oscillator Potential is given by the following equations:

$$V(\tilde{r}) = \frac{1}{2}m_Q\omega^2\tilde{r}^2 \tag{39}$$

$$\omega = \frac{1}{2}(M_{2s} - M_{1s})$$

It is worth mentioning that this is the most simple choice, leading to a Gaussian shape wave function as given in Figures 9 and 10. The analytic solution for the Schrödinger equation is:

$$u(\tilde{r}) = \exp -\frac{1}{4}m_Q\omega\tilde{r}^2 \tag{40}$$

On the other hand, another potential is chosen and known in the literature as Buchmüller-Tye Potential. It has a Coulomb-like behaviour and it is effective at a small size of $\tilde{r}$.

$$V(\tilde{r}) = \frac{k}{\tilde{r}} - \frac{8\pi}{27}\frac{\upsilon(\lambda\tilde{r})}{\tilde{r}} \tag{41}$$

for $\tilde{r} \geq 0.01$ fm. And

$$V(\tilde{r}) = -\frac{16\pi}{25}\frac{1}{\tilde{r}\ln(\omega(\tilde{r}))} \times \left(1 + 2\left(\gamma_E + \frac{53}{75}\right)\frac{1}{ln(\omega(\tilde{r}))} - \frac{462}{625}\frac{\ln(\ln(\omega(\tilde{r})))}{\ln(\omega(\tilde{r}))}\right) \tag{42}$$

for $\tilde{r} < 0.01$ fm. In this selection it is given:

$$\omega(\tilde{r}) = \frac{1}{\lambda_{MS}^2\tilde{r}^2}$$

$$\lambda_{MS} = 0.509GeV$$

$$k = 0.153GeV^2$$

$$\lambda = 0.406GeV$$

where $\gamma_E = 0.5772$ is the Euler constant.

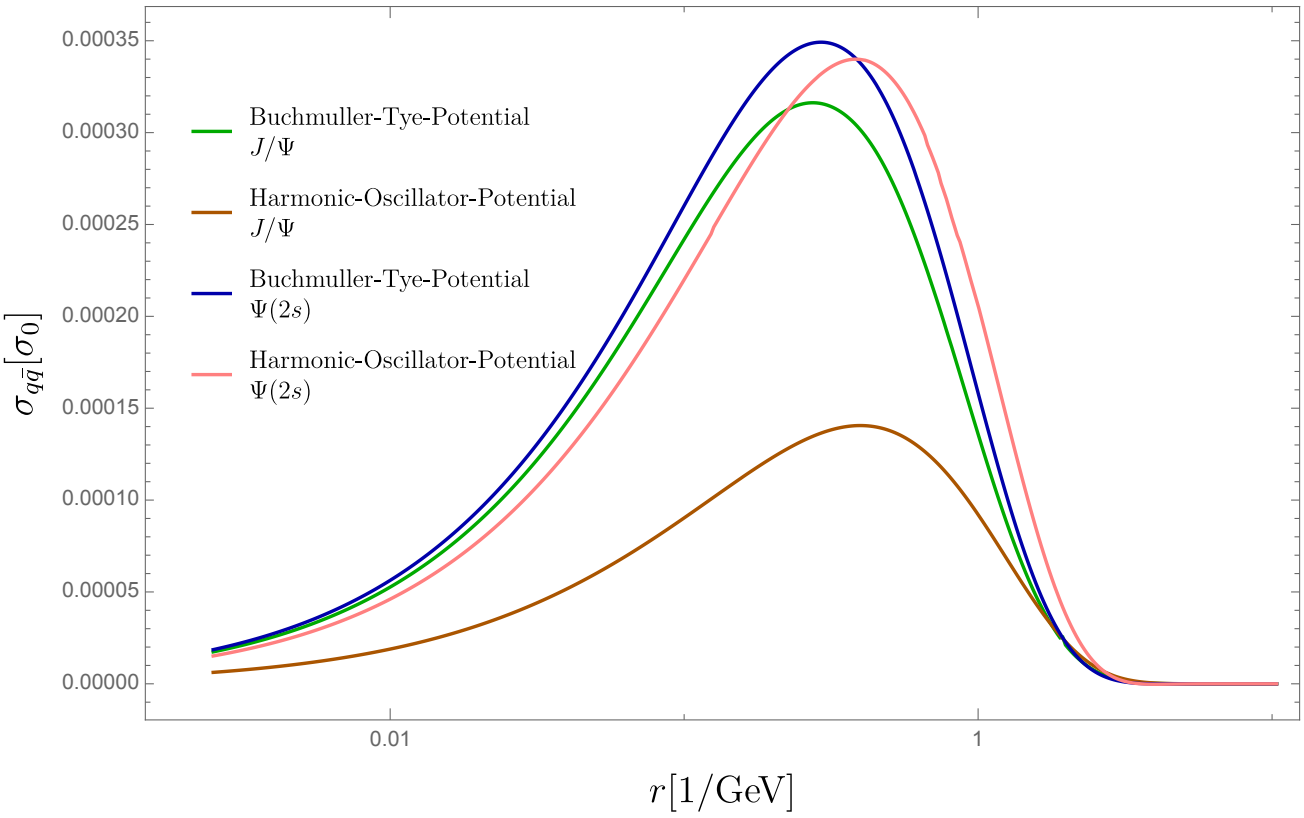


Figure 9: $J/\Psi$ Dipole cross section for the quark-antiquark pair for the LC-wavefunctions solutions for different potential with the parameters given in [22] as a function r. The distribution function $\Psi_V(r,z)$ is generated by two models for the $b-b^-$ interaction potential: Harmonic Oscillator Model and the Buchmüller-Tye Parameterisation.

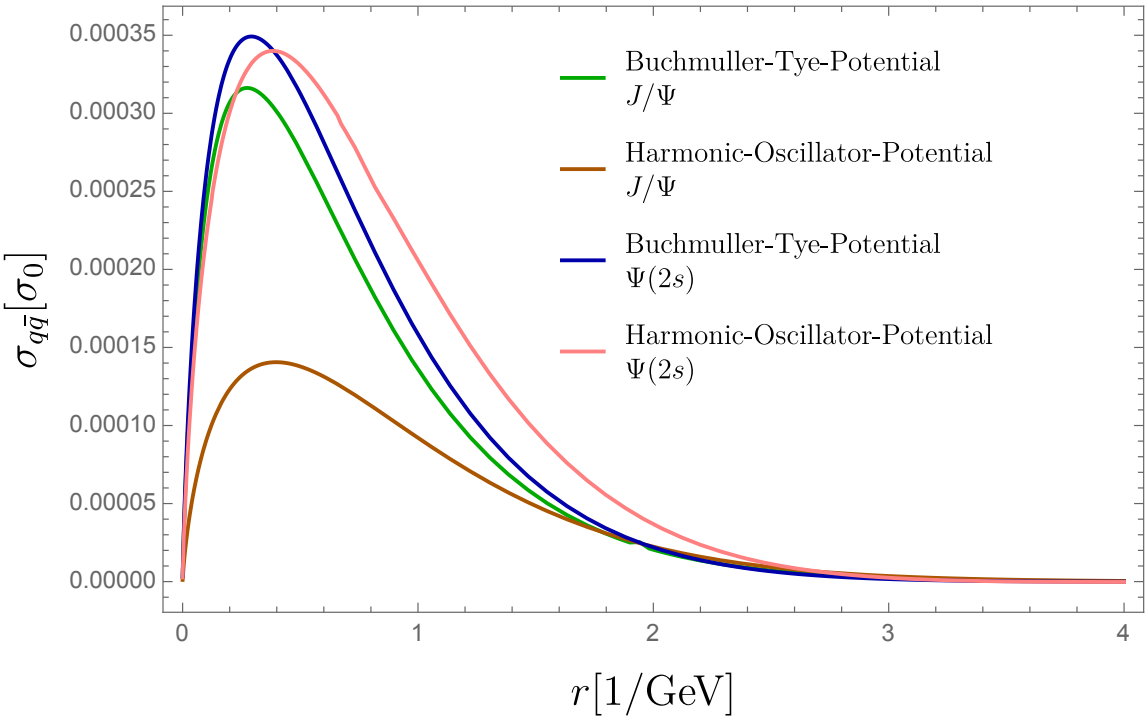


Figure 10: $\Psi(2s)$ Dipole cross section for the quark-antiquark pair for the LC-wavefunctions solutions for different potential with the parameters given in [22] as a function r. The distribution function $\Psi_V(r,z)$ is generated by two models for the $b-b^-$ interaction potential: Harmonic Oscillator Model and the Buchmüller-Tye Parameterisation.

### 4.3.2 Gaussian wave-functions

In order to verify if the saturation effects strongly depend on the wave function implemented, another kind of them was used. This kind of wave function is known in the literature as **Gaussian Wave Functions**. According to [28] the simplest way of modelling a vector meson wave function is to assume that is predominantly a quark-antiquark state and that the spin and polarisation are the same as the photon. Furthermore, the transversely polarised vector meson wave function is equal to:

$$\Psi^V_{h\bar{h},\lambda=\pm1}(r,z) = \pm\sqrt{2N_c}\frac{1}{z(1-z)}\left[ie^{\pm i\theta_r}[z\delta_{h,\pm}\delta_{\bar{h},\mp} - (1-z)\delta_{h,\mp}\delta_{\bar{h},\pm}]\partial_r + m_f\delta_{h,\pm}\delta_{\bar{h},\mp}\right]\Phi_L(r,z) \tag{43}$$

The longitudinally polarised wave function is more complicated because the decoupling of the quarks to the meson is non-local and its given by:

$$\Psi^V_{h\bar{h},\lambda=0}(r,z) = \sqrt{N_c}\delta h, -\bar{h}\left[M_V + \delta\frac{m_f^2 - \nabla_r^2}{M_V z(1-z)}\right]\Phi_L(r,z) \tag{44}$$

where $\nabla_r^2 \equiv (1/r)\partial_r + \partial_r^2$ and $M_V$ is the meson mass. Now, [28] state that where the photon and vector meson wave functions overlap is given by:

$$(\Psi_V^*\Psi)_T = \hat{e}_f e\frac{N_c}{\pi z(1-z)}\{m_f^2 K_0(\epsilon r)\phi_T(r,z) - [z^2 + (1-z)^2]\epsilon K_1(\epsilon r)\partial_r\phi_T(r,z)\} \tag{45}$$

and

$$(\Psi_V^*\Psi)_L = \hat{e}_f e\frac{N_c}{\pi}2Qz(1-z)K_0(\epsilon r)\left[M_V\phi_L(r,z) + \delta\frac{m_f^2 - \nabla_r^2}{M_V z(1-z)}\phi_L(r,z)\right] \tag{46}$$

where the effective charge $\hat{e}_f = 2/3$ for $J/\Psi$ meson.

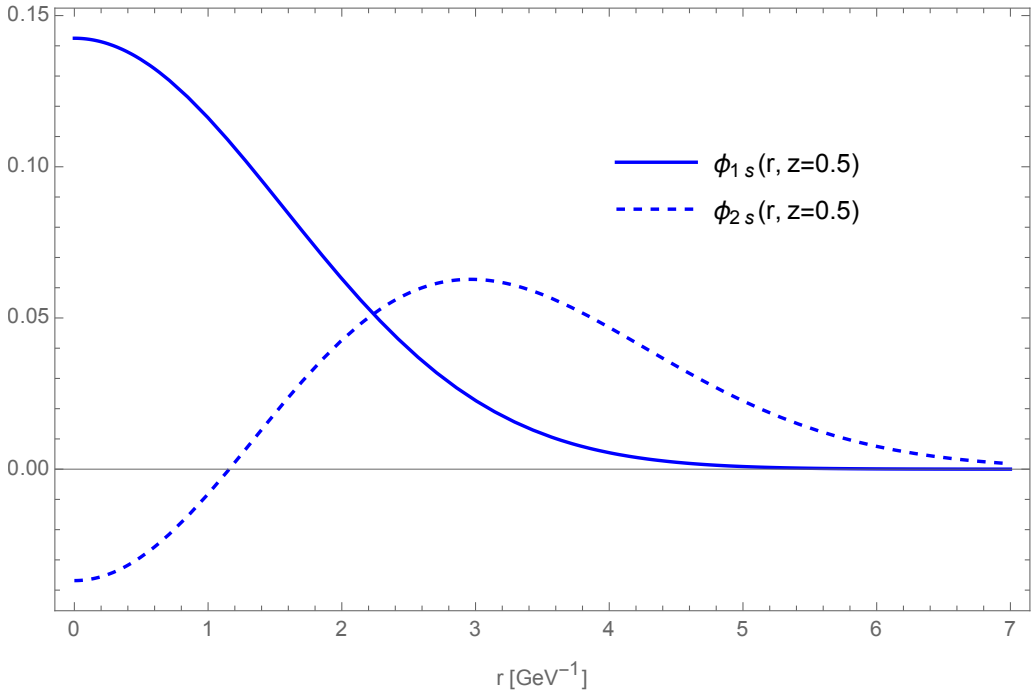


Figure 11: The Gaussian wave function $\Psi_V(r,z)$ for the two vector mesons $J/\Psi$, and $\Psi(2s)$ respectively, for the same quark momentum fractions $z$.

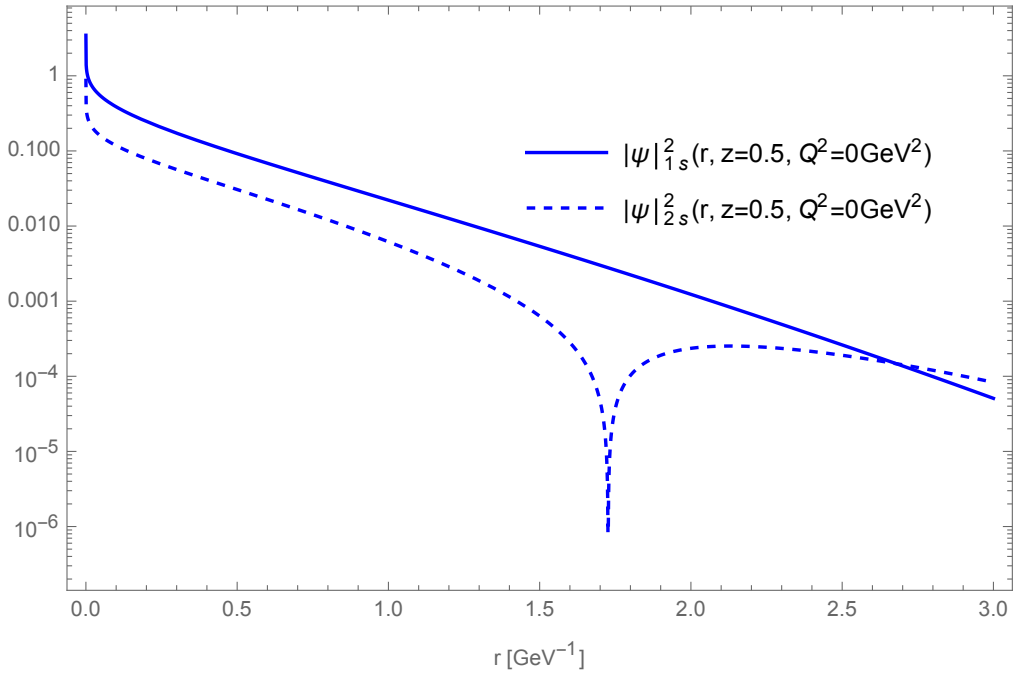


Figure 12: The Gaussian squared wave function $\Psi_V^2(r, z)$ for the two vector mesons $J/\Psi$, and $\Psi(2s)$ respectively, for the same quark momentum fractions $z$ and the region $Q^2 = 0$.

## 4.4 Dipole Models

Is of particular interest to describe the inclusive and diffractive deep inelastic scattering cross sections in HERA and LHC detectors. A useful tool to do that, are the well-known dipole models due to the fact they provide an elegant description of QCD reactions at low-x and low $Q^2$ region. [22] Also because it allows describing simultaneously a bunch of physical reactions; such as deep inelastic scattering processes, inclusive diffractive processes, exclusive $J/\Psi$, $\rho$, and $\Phi$ production, diffractive jet production, and finally, diffractive or non-diffractive charm production. The optical theorem boldly relates all these processes with their gluon density which is the same for all of them. [22] If it is needed to determine with high accuracy the gluon densities, it is needed need to rely on the analysis of high quality, inclusive deep inelastic scattering taken from the experimental data available in $x$ and $Q^2$ region. Therefore, H1, ZEUS, ALICE and LHCb are ideal experiments for our study because they have combined inclusive deep inelastic scattering cross-sections to reduce the

errors and increase the precision by a factor of two. [22]

The new kinematic region of small values of the Bjorken variable $x$ directly relates to the Regge limit in QCD. In this limit, QCD enters the semi-hard perturbative domain where $x \approx Q^2/W^2 \ll 1$ and the virtual photon mass $Q$ is much bigger than the Lagrangian $\mathcal{L}_{QCD}$ and simultaneously, smaller than the invariant energy of the virtual photon-proton system, $W$. All of these, guarantee that $\alpha_s(Q)$ is small enough for perturbative calculations to apply to the system. It has a great advantage because it leads to either DGLAP or the BFKL evolution equations. [25] It is required to answer the question of whether we still get a precise description of HERA and LHC data with the saturation model and its modification.

Before starting, let's define some scales:

- $\sqrt{s}$: Center of mass energy because of the reaction of the electron and the hadron
- $W^2$: Center of mass energy because of the reaction of the photon and the hadron
- $Q$: Resolution of the insides of the hadrons $1/\lambda$

Mathematically, the centre of mass energy and the resolution are put together to define a new variable $x$. It is worth mentioning that these two quantities are defined in terms of their momentum.

$$W^2 = (p+q)^2$$

$$s = (k+p)^2$$

$$x = \frac{Q^2}{(W^2+Q^2)} = \frac{Q^2}{2pq}$$

$$W^2 = (p+q)^2 = p^2 + 2pq + q^2 = 0 + 2pq - Q^2$$

Where the limit $p = 0$ is implemented. Finally,

$$\frac{1}{x} = \frac{W^2+Q^2}{Q^2}$$

**Dipole Models** have presented a radical new way of understanding the deep inelastic scattering process, dividing it into a two-stage process; First, the virtual photon fluctuates into a dipole of quark and anti-quark pair, and secondly, the dipole interacts with the proton.

[30] The dipole presents a quasi-stable quantum mechanical state with a considerably long lifetime of the order of $Q^2 \sim 1/m_p x$ with the size of $r$ and has the characteristic of remaining unchanged during the scattering. Now, to determine the probability of finding a dipole of size $r$ within a photon that only depends on the value of the external $Q^2$ and the fraction of the photon momentum carried by the dipole formed by a pair of quarks, a wave-function $\Psi$ is implemented. The scattering amplitude will be defined as the product of the virtual photon wave function $\Psi$ and the dipole cross-section $\sigma_{dip}$. It determines the probability of the scattering of the dipole-photon process. [30]

Before defining the dipole models implemented in this study, is worth mentioning that this study aims to explore the energy dependence of the cross-section for exclusive photo-production of vector mesons $J/\Psi$ and its excited state $\Psi(2s)$ so possible signs for the onset of non-linear QCD dynamics can be found. Therefore, the saturation models were studied for both the linear regime where saturation effects in the nuclei are absent, and for the complete version where saturation effects in the nuclei are considered. All of this is so we can have an accurate description of the gluonic distributions subject to both linear and nonlinear evolutions.

## 4.5 GBW Model

It is a simple ansatz dipole model able to describe the total inclusive and diffractive cross-sections. The cross-section for a vector meson production is given by the Golec-Biernat and Wuesthoff model (GBW saturation model) (see [22]) and its modification to cover high values of $Q^2$, which takes into account the gluon density in an explicit way. The dipole cross-section of the GBW model is given by:

$$\sigma_{dip}(r, x) = \sigma_0 \left(1 - exp\left[-\frac{r^2 Q_s^2(x)}{4}\right]\right) \tag{47}$$

The r corresponds to the transverse separation between the quark and the antiquark, and x is the dependent scale parameter where the saturation scale $Q_s$ is defined as [22].

$$Q_s^2(x) = Q_0^2 \left(\frac{x}{x_0}\right)^{-\lambda} \tag{48}$$

with $Q_0^2 = 1$ GeV. The above cross-section has a property of geometric scaling [22]:

$$\sigma_{dip}(r, x) = \sigma_{dip}\left(rQ_s(x)\right) \tag{49}$$

This means it becomes a function of a single variable, $rQs$, for all values of $r$ and $x$. The three parameters of this fit are $\sigma_0$, $\lambda$ and $x_0$. Another fact about the GBW model is that not incorporate QCD evolution in the resolution scale $Q^2$ in the small r part of the dipole cross-section [22]. It implies that the power $\lambda$ controls the growth of the total and diffractive cross-section with $x$ and is independent of $Q^2$. $\sigma_0$ is the constant that describes the value where the dipole cross-section saturation stabilizes. It provides a good description of data from medium $Q^2$ values, down to low values (From 30 GeV to 0.1 GeV). [22] [30] It is needed to fit the GBW model parameters to get the precision we want for the description of the data extracted from HERA and the LHC. That will be done by the Golec-Biernat Sapeta Fit in short displayed.

In summary, the GBW model is accurate in describing HERA and LHC data for small and moderate values of $Q^2$ thanks to the concept of parton saturation and using only three fitted parameters [22]. In conclusion, this model describes the grand qualities of the HERA experiment working with small and moderate values of $Q^2$ and with the transitions of the DIS structure functions for small values of $Q^2 \leq 1GeV^2$ which is possible to have with the addition of parton saturation and exclusively three parameters, preferably fixed if possible.

For this dipole model, two modifications were made: Firstly, an exponential expansion for the non-linear version was made (equation 47) leaving the following equation:

$$\sigma_{dip}(r, x) = \sigma_0 \left[\frac{r^2 Q_s^2(x)}{4}\right] \tag{50}$$

This was done to compare at which point the phase space region is separated from low and from saturated gluon densities. The growth of our theoretical prediction when it's in its linear version depends only on the saturation scale. Nevertheless, it was found that differences

between linear and non-linear implementations were relatively small at the level of photo-production cross-sections, in particular, if both theoretical and experimental uncertainties are taken into account.

Finally, for this study, a parameter $k$ was introduced in order to vary the strength of non-linear corrections in the dipole model. This parameter does not affect the linear result, but it tells us how important are the non-linear corrections. In particular, if this parameter $k$ is too big, the non-linear terms become relevant, and then if it is close to zero, everything also becomes zero. For the non-linear version, the dipole cross-section is given by:

$$\sigma_{dip}(x, r^2, k) = \frac{\sigma_0}{k}\left(1 - \exp\left[-k \cdot \frac{r^2 Q_s^2(x)}{4}\right]\right) \tag{51}$$

where equation (48) is again the scale that grows with the energy. (As $x \to 0$) Finally, when making the exponential expansion of equation (51), the $k$ term gets cancelled with the $k$ in the denominator and we have again our linear version of the dipole model as in equation (50) in which saturation effects are not considered.

$$\sigma_{dip}(x, r^2, k) = \sigma_0\left[\frac{r^2 Q_s^2(x)}{4}\right] \tag{52}$$

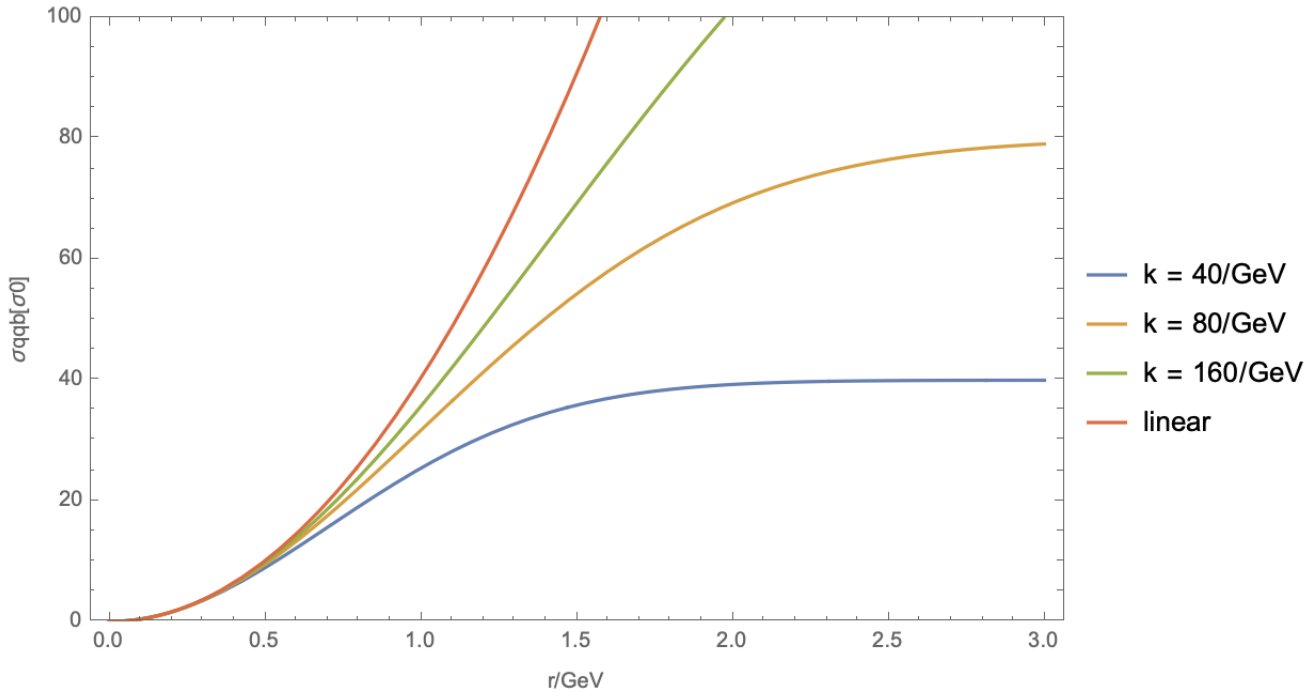


Figure 13: Dipole cross section for the $J/\Psi$ vector meson given by the GBW model for the scale with the parameters from fit GBS explained in [23] as a function r implementing the parameter $k$ previously explained to vary the strength of non-linear corrections in the dipole model.

## 4.6 BGK Model (DGLAP Improved Model)

For this study, another dipole model was implemented. This model is an improved version of the GBW model, because takes into account the DGLAP evolution of the gluon density in an explicit way [30]. One of the advantages of this model is that it also takes into account the eikonal approximation of the GBW model when saturation occurs. The total cross-section for a vector meson production is given by the Bartels, Golec-Biernat and Kowalski model (BGK model):

$$\sigma_{dip}(x, r^2) = \sigma_0 \left(1 - \exp\left[-\frac{\pi^2 r^2 \alpha_s(\mu^2) x g(x, \mu^2)}{3\sigma_0}\right]\right) \tag{53}$$

Where $\alpha_s(\mu^2)$ is the strong coupling constant, $g(x, \mu^2)$ is the gluon distribution in the proton subject to DGLAP evolution, $r$ the dipole size, x a scale defined by $M^2/W^2$ and $\sigma_0$ is a

constant.

At this point, two different fits can be implemented for the dipole model given in equation (53): the fit given by the authors of [30] and the fit given by the authors in [22]. Despite the fact in the section on results the fit described in [30] was implemented; for practical purposes and because the gluon distribution extracted from this paper didn't differentiate between linear and non-linear effects, only the fit discussed by the authors in [22] will be described. Back to equation (53), the term $g(x, \mu^2)$ denotes the gluon distributions taken from the scale:

$$\mu^2 = \frac{C}{r^2} + \mu_0^2 \tag{54}$$

According to [22], the gluon distribution evolves following the DGLAP evolution equations truncated to the gluonic sector as follows:

$$\frac{\partial g(x,\mu^2)}{\partial \ln \mu^2} = \frac{\alpha_s(\mu^2)}{2\pi} \int_x^1 \frac{dz}{z} P_{gg}(x) g(\frac{x}{z}, \mu^2) \tag{55}$$

From the initial condition,

$$xg(x, Q_0^2) = A_g x^{-\lambda_g} (1-x)^{5.6} \tag{56}$$

taken at the scale $Q_0 = 1$ GeV. The authors in [23] used the power 5.6 because it regulates the large-x behaviour and it's motivated by global fits to deep inelastic scattering data with the LO DGLAP equations. The splitting function $P_{gg}$ contains real and virtual terms with the number of active quark flavours $n_f$ and is given by:

$$P_{gg}(z) = 2N_c \left( \frac{z}{(1-z)_+} + \frac{1-z}{z} + z(1-z) \right) + \delta(1-z) \frac{11C_A - 4n_f T_R}{6} \tag{57}$$

Where $C_a = N_c = 3$ and $T_R = 1/2$. The authors in [22] set in the leading order of the strong coupling constant $\Lambda = 300$ MeV; this implies that BGK model will have five parameters to fit: $\sigma_0$, $A_g$, $\lambda_g$, $C$ and $\mu_0^2$.

The dipole cross-section given by equation (53) has the property of colour transparency and tends to the perturbative QCD result in the limit $r \to 0$. Furthermore, for small-size dipoles, the scale $\mu^2 \approx C/r^2$ and the dipole cross-section is proportional to $r^2$ next to the logarithmic modifications due to the scale dependence of the gluon distribution: [22].

$$\sigma_{dip} \approx \frac{\pi^2}{3} r^2 \alpha_s(C/r^2) x g(x, C/r^2) \tag{58}$$

These extra logarithms allow better fits to the data at large values of $Q^2$. When the limit of large dipoles $\mu^2 \approx \mu_0^2$ and as consequence, the dipole cross section will be equal to:

$$\sigma_{dip} \approx \sigma_0 \left[1 - \exp\left[-\frac{\pi^2 r^2 \alpha_s(\mu_0^2) x g(x, \mu_0^2)}{3\sigma_0}\right]\right] \tag{59}$$

Therefore, when having $r$ large, the GBW dipole cross-section with its saturation scale is given by:

$$Q_s^2(x) = \frac{4\pi^2}{3\sigma_0} \alpha_s(\mu_0^2) x g(x, \mu_0^2), \tag{60}$$

where the $x$ gives a dependency by the gluon distribution taken because of the scale $\mu_0^2$. [22]. The equation (53) is a geometric scale for this specific equation. The features of the dipole cross-section can also be obtained by having a different scale $\mu$:

$$\mu^2 = \frac{\mu_0^2}{1 - exp(-\mu_0^2 r^2 / C)} \tag{61}$$

and the interpolation is subtle between in the term $C/r^2$ behaviour when having a small $r$ and the constant $\mu^2 = \mu_0^2$ when $r \to \infty$. In short, the BGK model extends the GBW model saturation to larger values of $Q^2$, giving a fantastic description of both HERA and LHC data up to $Q^2 = 650\ GeV^2$ achieved by modifying the dipole cross-section for small sizes to match the perturbative QCD results in this region. At last but not least, both characteristics of the GBW model that are the saturation scale and geometric scaling are conserved in the BGK model in the region of $rQ_s > 1$. This is useful because they are responsible for the transition of $F_2$ to small values of $Q^2$ [22].

As it was done for the GBW model, an exponential expansion was done for equation (53) leading to the following equation:

$$\sigma_{dip}(x, r^2) = \sigma_0 \left[\frac{\pi^2 r^2 \alpha_s(\mu^2) x g(x, \mu^2)}{3\sigma_0}\right] \tag{62}$$

This expansion was made to explore the difference between linear and non-linear effects where the linearized version does not take into account saturation effects and the non-linear version does take into account saturation effects.

The growth of the theoretical prediction despite the fact is in its linear version, takes into account DGLAP evolution in the description. Nevertheless, it was found that differences

between linear and non-linear implementations were relatively small at the level of photo-production cross-sections, in particular, if both theoretical and experimental uncertainties are taken into account such as in the GBW model.

On the other hand, a modification to the non-linear version was made for the BGK model. This modification consists in implementing a parameter $k$ as it was done for the GBW model which simulates non-linear effects through exponentiating of the leading order QCD description. The modified model has the following form:

$$\sigma_{dip}(x, r^2, k) = \frac{\sigma_0}{k}\left(1 - \exp\left[-k \cdot \frac{\pi^2 r^2 \alpha_s(\mu^2) x g(x, \mu^2)}{3\sigma_0}\right]\right) \tag{63}$$

Since this model is not as simple as the GBW, for obtaining the linear version of the modified BGK model a rather tedious process was made. Firstly, the numerical values of dipole cross sections and structure functions corresponding to the fits given by [22] were taken and interpolated. After that, the value for the linear version without the modification was obtained by expanding the exponential as it was done in equation (62). The last step was to calculate the linearized version using a small $k$. The explicit linear version of the modified model has the following form:

$$\sigma_{dip}(x, r^2, k) = \frac{\sigma_0}{k}\left[1 - \left(1 - \frac{\pi^2 r^2 \alpha_s(\mu^2) x g(x, \mu^2)}{3\sigma_0}\right)^{\frac{\sigma_0}{\frac{\sigma_0}{k}}}\right] \tag{64}$$

Therefore, assuming this premise that $k$ is small enough, the linear version appears for the BGK model: (as in equation 62)

$$\sigma_{dip}(x, r^2, k) = \sigma_0\left[\frac{\pi^2 r^2 \alpha_s(\mu^2) x g(x, \mu^2)}{3\sigma_0}\right] \tag{65}$$

The $k$ parameter does not affect the linear result, but it tells how important are the non-linear corrections. In particular, if this parameter k is too small, the non-linear terms become relevant, then if it is close to zero, everything also becomes zero, and finally, if it approaches one, it causes no hierarchy and the importance of terms is only determined by the saturation scale.

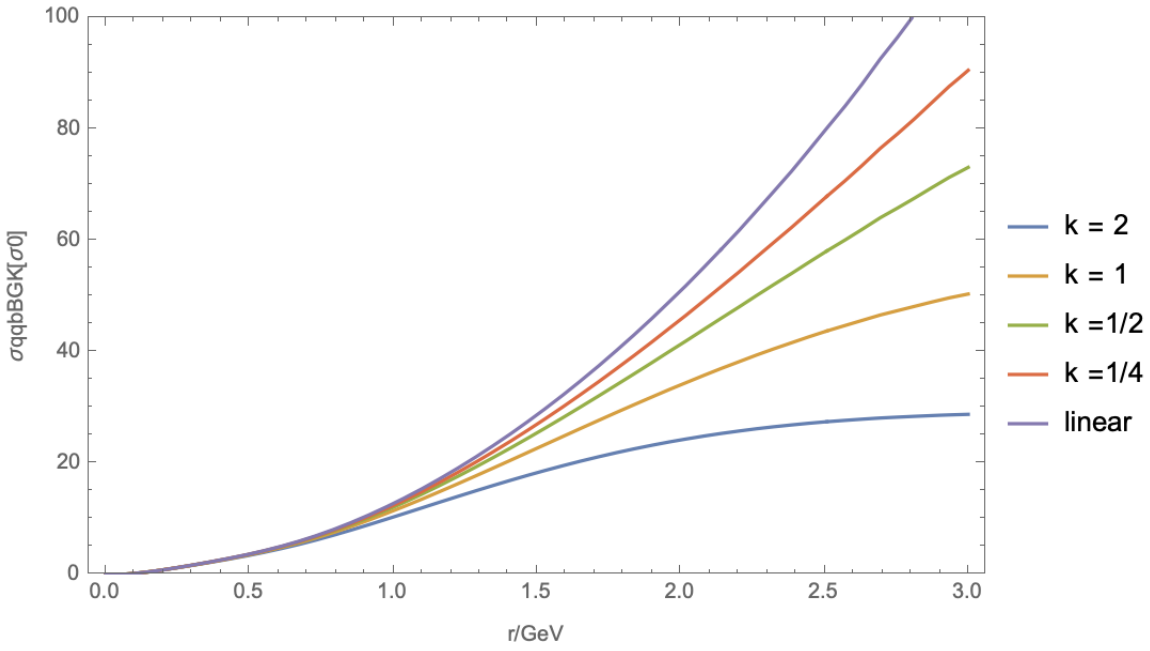


Figure 14: Dipole cross section for the $J/\Psi$ vector meson given by the BGK model for the scale with the parameters from fit GBS explained in [23] as a function r implementing the parameter $k$ previously explained to vary the strength of non-linear corrections in the dipole model.

## 4.7 Exclusive Photo-production of $J/\Psi$ and $\Psi(2s)$ as a tool to explore the transition to high and saturated gluon densities at the LHC.

The exclusive photo-production of vector mesons is the main concern of this research due to the fact this observable is very useful for describing the gluon distribution at low $x$ ($x = 4 \times 10^{-6}$). [25] Charm quarks are of special interest because they provide a hard scale at the limit between soft and hard physics. As a consequence of that, it is expected for this observable to be sensitive to the presence of a semi-hard scale; which is directly associated with the transition to the saturation region. On the other hand, it is worth mentioning that the light-cone wave functions differentiate their dependency on their dipole size between the base state and the excited state of the charmounium-bound state. To study the gluon

distribution at LHC for the process:

$$\gamma(q) + p(p) \rightarrow V(q') + p(p') \tag{66}$$

data was extracted from both HERA and LHC to study the photo-production of the bound states of the charms quarks (In this case, the $J/\Psi$ particle and the $\Psi(2s)$), where $V = J/\Psi$, $\Psi(2s)$, and $\gamma$ denotes the virtual photon. [25]
There are three main objectives of this research project:

1. The study of the exclusive photo-production of vector mesons at the Large Hadron Collider.

2. Determination of the photoproduction cross-section and comparison with data.

3. Identify observables that can distinguish between gluon distributions subject to linear and non-linear QCD evolution.

The Feynman diagrams that describe the photo-production of vector mesons are given by the following figures:

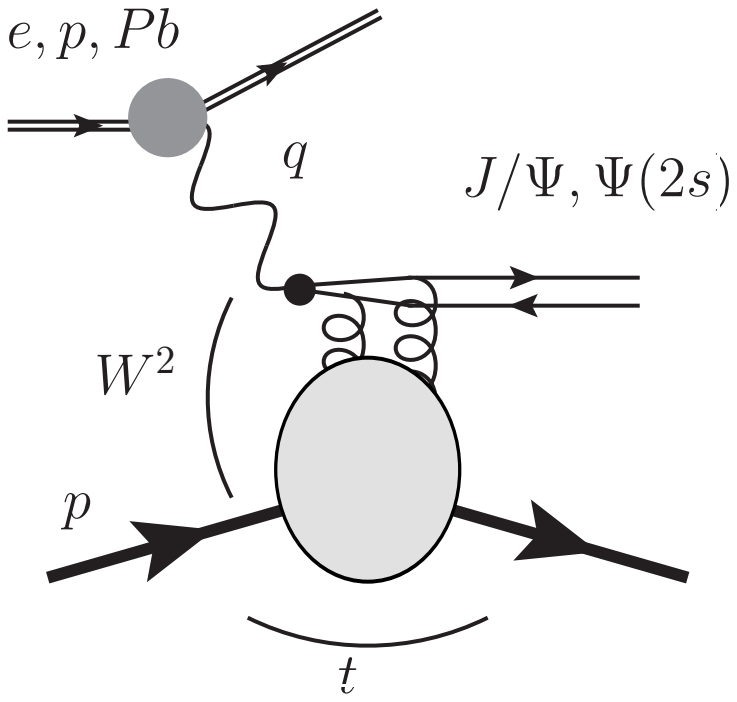


Figure 15: An ultra-peripherical collision occurring between a hadron and an ultra-heavy lead atom, (it can be also an electron or proton) where they are exchanging a photon with momentum q and creating a dipole of quarks, resulting in a vector meson. t is the momentum transfer $t = (q - q')$ and $W^2 = (q + p)^2$ is the squared center-of-mass energy. [25] (Hentschinski and Padron, 2021)

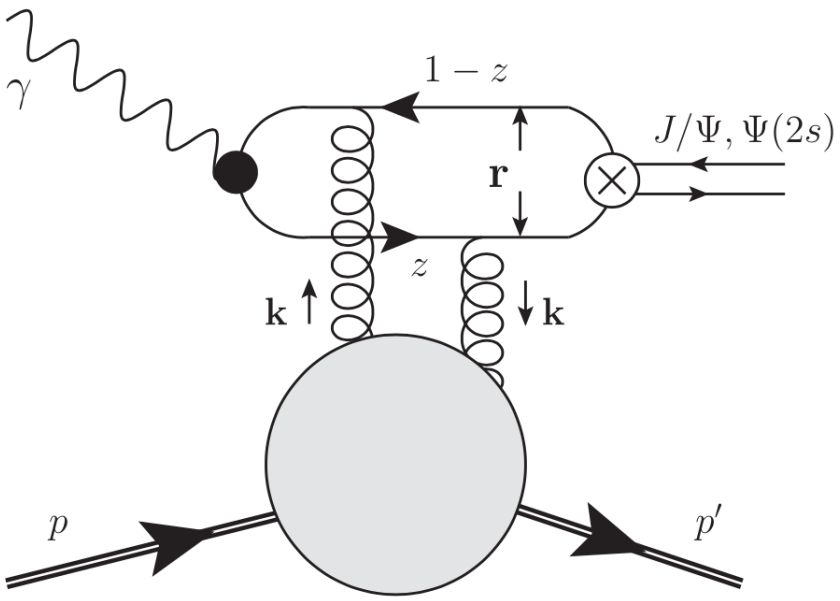


Figure 16: Zooming in the section of the dipole of quarks of the previous figure, we get the following Feynman diagram for the quark-antiquark dipole, where the quasi-real photon has virtuality $Q \to 0$, and momentum fractions this latter has been given by $z$ and $1 - z$. The transverse separation is given by $r$. Finally, $k$ denotes the transverse momentum transmitted from the unintegrated gluon distribution of the proton which is represented as a grey bolb. [25] (Hentschinski and Padron, 2021)

The differential cross section for the exclusive photo-production of a vector meson according to [25] is given by:

$$\frac{d\sigma}{dt}(\gamma p \to Vp) = \frac{1}{16\pi} \mid A_T^{\gamma p \to Vp}(W^2, t) \mid \tag{67}$$

Where $A_T(W^2, t)$ is the scattering amplitude for the reaction $(\gamma p \to Vp)$ for colour singlet exchange in the t-channel, with an overall factor $W^2$ already extracted. [25]
Now, we must calculate the total photo-production cross-section based on the dipole. This is only possible if one follows a two step process:

1. Determine the differential cross-section at zero momentum transfer $(t = 0)$
2. Model the t-dependence, because this would allow us to relate the differential cross-section at $t = 0$ to the integrated cross-section.

We must assume that the differential cross section has an exponential drop-off with $\mid t \mid$ as follows:

$$\sigma \sim exp[- \mid t \mid B_D(W)] \tag{68}$$

With an energy dependent t slope parameter $B_D$:

$$B_D(W) = \left[ b_0 + 4\alpha' \ln\left(\frac{W}{W_0}\right)\right] GeV^{-2} \tag{69}$$

Therefore, the total cross-section for vector meson production is given as follows:

$$\sigma^{\gamma p \to Vp}(W^2) = \frac{1}{B_D(W)} \frac{d\sigma}{dt}(\gamma p \to Vp) \mid_{t=0} \tag{70}$$

The uncertainty introduced through the modelling of the t-dependence mainly affects the overall normalization of the cross-section with a mild logarithmic dependence on the energy. [25]

Now, is necessary to calculate the scattering amplitude so we can obtain our cross-section. In order to calculate it, we first note that the dominant contribution is provided by its imaginary part. Corrections due to the real part of the scattering amplitude can be estimated using dispersion relations, in this case: [25]

$$\frac{\Re eA(W^2,t)}{\Im mA(W^2,t)} = \tan\left(\frac{\lambda\pi}{2}\right) \tag{71}$$

with

$$\lambda(x) = \frac{d}{d\ln(1/x)} \ln \Im mA(x,t)$$

We do not assume $\lambda$ is a constant but instead determine the slope $\lambda$ directly from the W-dependent imaginary part of the scattering amplitude because the slope parameter $\lambda$ on energy $W$ gives us a reasonable correction to the $W$ dependence of the total cross-section. It is not assumed that $\lambda$ is constant, as a result the slope of $\lambda$ is obtained directly from the $W - dependent$ imaginary part for the scattering amplitude. [25] The imaginary part of the scattering amplitude is obtained using a Gaussian model for the light-cone wave function of the vector mesons and uses instead a re-fined description which includes relativistic spin-rotation effects in the forward limit. The imaginary part of the scattering amplitude is then:

$$\Im mA_T(W^2, t=0) = \int d^2\mathbf{r} \left[ \sigma_{q\bar{q}}\left(\frac{M_V^2}{W^2}, r\right) \overline{\Sigma}_T^1(r) + \frac{d}{dr}\sigma_{q\bar{q}}\left(\frac{M_v^2}{W^2}, r\right) \overline{\Sigma}_T^{(2)}(r)\right] \tag{72}$$

with $r =\mid \mathbf{r} \mid$. [25]
The functions $\overline{\Sigma}_T^{(1,2)}$ describe the transition of a transversely polarized photon into a vector meson V. These equations are given by:

$$\overline{\Sigma}_T^{(i)}(r) = \hat{e_f}\sqrt{\frac{\alpha_{e.m.}N_c}{2\pi^2}}K_0(m_f r)\Xi^{(i)}(r), i = 1, 2 \tag{73}$$

where

$$\Xi^{(1)}(r) = \int_0^1 dz \int_0^\infty dpp J_0(p \cdot r) \times \frac{m_T^2 + m_T m_L - 2p^2 z(1-z)}{m_T + m_L}\Psi_V(z, p) \tag{74}$$

$$\Xi^{(2)}(r) = \int_0^1 dz \int_0^\infty dpp^2 J_1(p \cdot r) \times \frac{m_T + m_L + m_T(1-2z)^2}{2m_T(m_T + m_L)}\Psi_V(z, p) \tag{75}$$

Where $\hat{e_f} = 2/3$ is the charge of the charm quark, $\alpha_{e.m}$ is the electromagnetic fine structure constant, $N_c = 3$ is the number of colors and $K_0$ with $J_{0,1}$ are the Bessel functions of the second and first kind respectively.
At last, $m_f$ is the quark charm's mass and $p =\mid \mathbf{p} \mid$ is the modulus of the transverse momentum. Therefore it is given that:

$$m_T^2 = m_f^2 + p^2 \tag{76}$$

and

$$m_L^2 = 4m_f^2 z(1-z) \tag{77}$$

for the wave function of the vector meson $\Psi_V(z, p)$. [12] [28] At last but not least, apart from determining the differential cross section for the $J/\Psi$ meson, it was also determined the radially excited charmonium $\Psi(2s)$ cross-section implementing as well as a set of charmonium wave functions given in [29] to estimate the uncertainties associated with the energy dependence of the LK and GBS fits given in [30] and [22] respectively.

The parameters for the diffractive slope $B_D$ as given in equation (69) take into account the following parameters determined from a fit to HERA data:

$$b_0^{(J/\Psi)} = 4.62 \tag{78}$$

$$b_0^{\Psi(2s)} = b_0^{J/\Psi} + 0.24$$

$$\alpha'_{(J/\Psi}(0) = 0.171 \tag{79}$$

$$\alpha'_{\Psi(2s)}(0) = \alpha'_{(J/\Psi} - 0.02$$

# 5. Results

The section of results will be divided into three parts:

The first part will implement the BGK saturation dipole model for predicting the energy dependence for the photo-production cross section using two different fits: the Luszczak-Kowalski fit (LK Fit) [30] and the Golec-Biernat-Sapeta Fit (GBS fit) [22]. Light-Cone wave functions were also implemented in this part of the study for solving the Schrödinger equations given in (32) and (37) with the Buchmüller-Tye potential. After all of this, the theoretical prediction will be compared with data extracted from both the LHC and HERA detectors data.

For the second part of the results, it was verified that the wave function implemented strongly affects the non-linear effects in the theoretical predictions. Alike section one, the same analysis was made for the BGK model but with two main differences: Firstly, the fit given in [30] was taken away and just left the GBS fit [22], due to the fact LK fit doesn't give a good description of the data. Secondly, the Gaussian wave functions given by [28] were implemented to verify if the saturation effects observed at low $x$ strongly depend on the chosen wave function, obtaining very satisfying results.

The third and last part of the study will present again the summarized results for two saturation dipole models: the BGK model and the GBW implementing for both the GBS fit found in [22] with a slight difference; a parameter $k$ was introduced in order simulate non-linear effects through exponentiating of the leading order QCD description. For this study, again the Gaussian wave functions were implemented [28].
The reason for implementing a $k$ parameter into our study is because is not entirely clear to

which extent HERA data can constrain non-linear corrections (because they are not large for the x values of HERA). That's why we are interested in what is the importance of these terms in the LHC. The parameter $k$ allows us to vary the strength of non-linear corrections in the dipole models. This parameter does not affect the linear result, but it tells us how important are the non-linear corrections.

Each of the theoretical predictions was compared to data extracted from both HERA and the LHC. It's important to mention that for every section we included three different plots; one for the energy dependency for the photo-production cross-section for $J/\Psi$ vector meson, another for the radially excited charmonium $\Psi(2s)$ and finally, one for the ratio of the photo-production cross-sections between $\Psi(2s)$ and $J/\Psi$ vector mesons cross sections. Since the ratio between cross sections enhance the difference between linear and non-linear evolution, it becomes a useful tool to distinguish between linear and non-linear QCD evolution as it was observed in [25].

Finally, it is worth saying that the measurement of the ratio of the photo-production cross-section is a useful tool to study because it cancels out errors in the normalization that the data and our model may have. Therefore, this observable could in principle apply to photon-proton scattering at the highest centre of mass energies as measured at LHC, as well as to photo-production cross-sections obtained in electron-ion scattering at the future Electron-Ion Collider.

## 5.1 Summarized results comparing LK and GBS fits implementing the BGK dipole saturation model

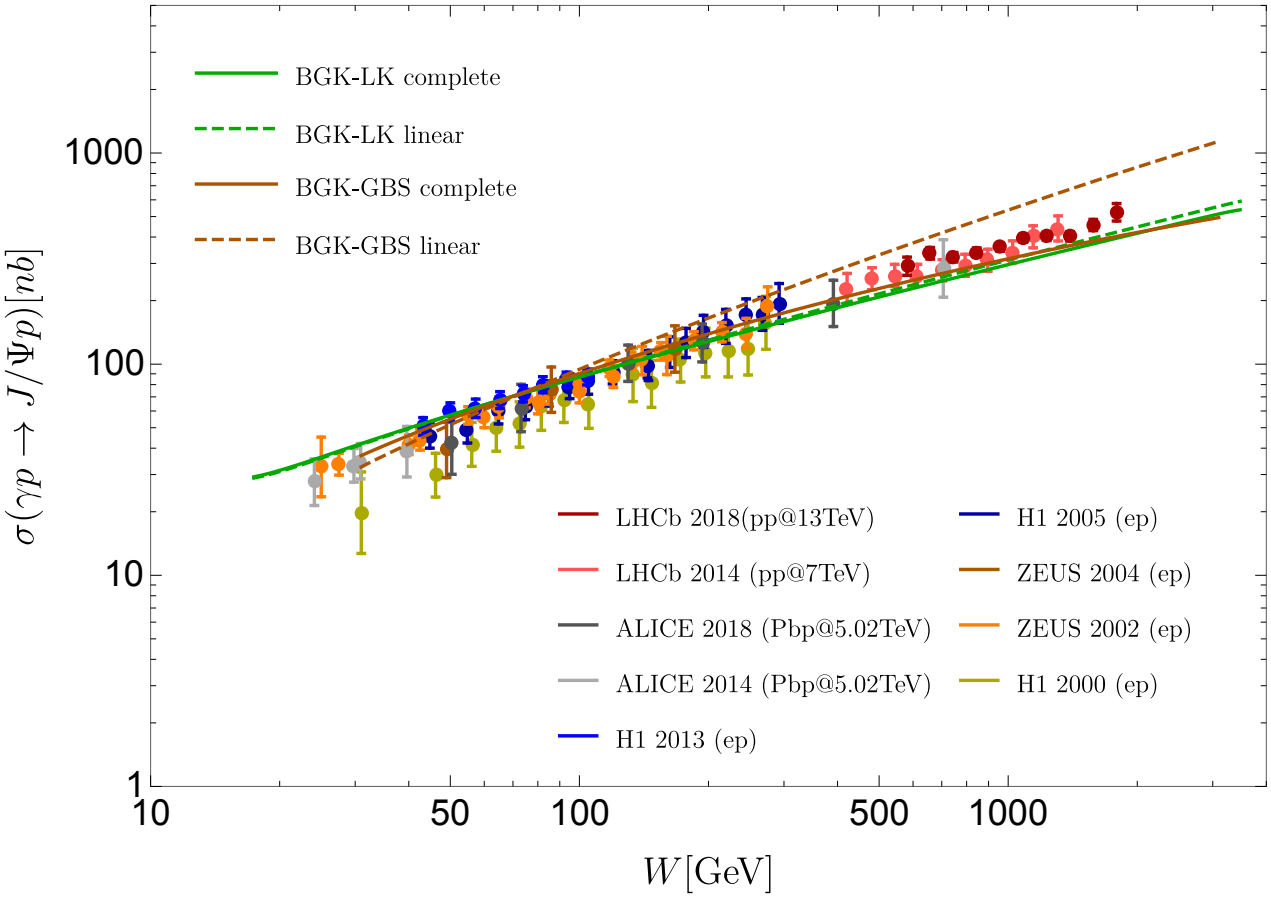


Figure 17: The energy dependence of the $J/\Psi$ photo-production cross-section as provided by the BGK saturation model for gluon distribution, considering two different fits: the LK and the GBS. (see [22] and [30]).

It is further displayed the photo-production data measured at HERA by ZEUS ([14],[15]) and H1 ([7],[8],[9]) as well as LHC data obtained from ALICE ([4],[6]) and LHCb ($W^+$ solutions) ([2],[3]) collaborations. The fit was made to the highest precision data extracted from LHCb collaboration and the error bars displayed in figure 17 do not denote the complete uncertainty associated with these data points.

It can be seen that the differences between linear and non-linear regimes for the LK fit are

almost null. Therefore, it is very probable that non-linear corrections strongly depend on the implemented fit. Specifically, for this first part the Buchmüller-Tye potential was chosen in order to give the numerical solution of the Schrödinger equation given by authors in [13].

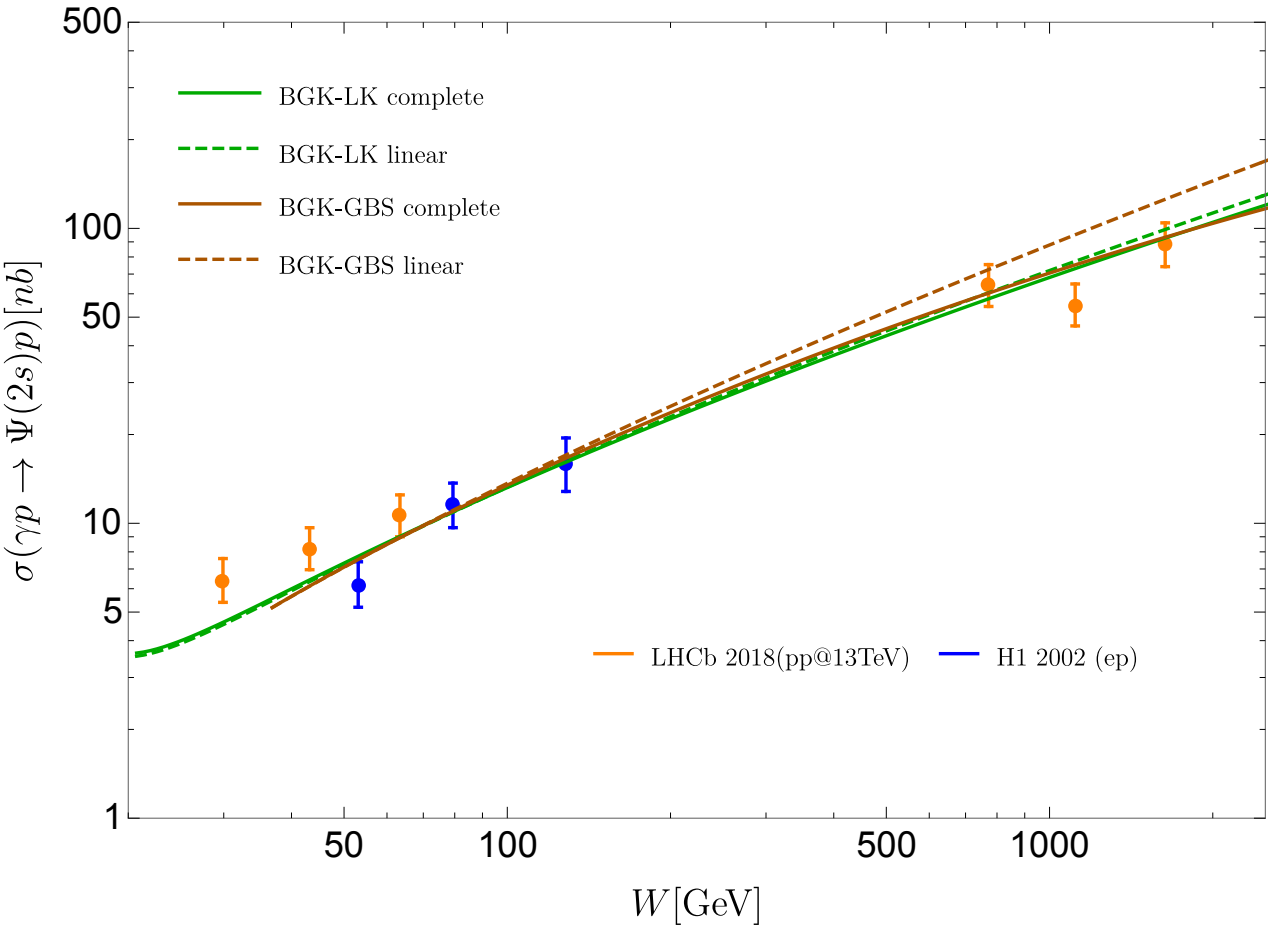


Figure 18: The energy dependence of the $\Psi(2s)$ photo-production cross-section as provided by the BGK saturation model for gluon distribution considering two different fits: the LK and the GBS. (see [22] and [30]).

It is further displayed the photo-production data measured at HERA by H1 ([7],[34]) as well as LHC data obtained from the LHCb collaboration ($W^+$ and $W^-$ solution) [3]. The dipole model provides a rather excellent description of the energy dependence with a very similar result for the wave functions given by authors in [29]. The Buchmüller-Tye potential was chosen to give the numerical solution of the Schrödinger equation, and finally, the fit was made to the highest precision data extracted from LHCb collaboration.

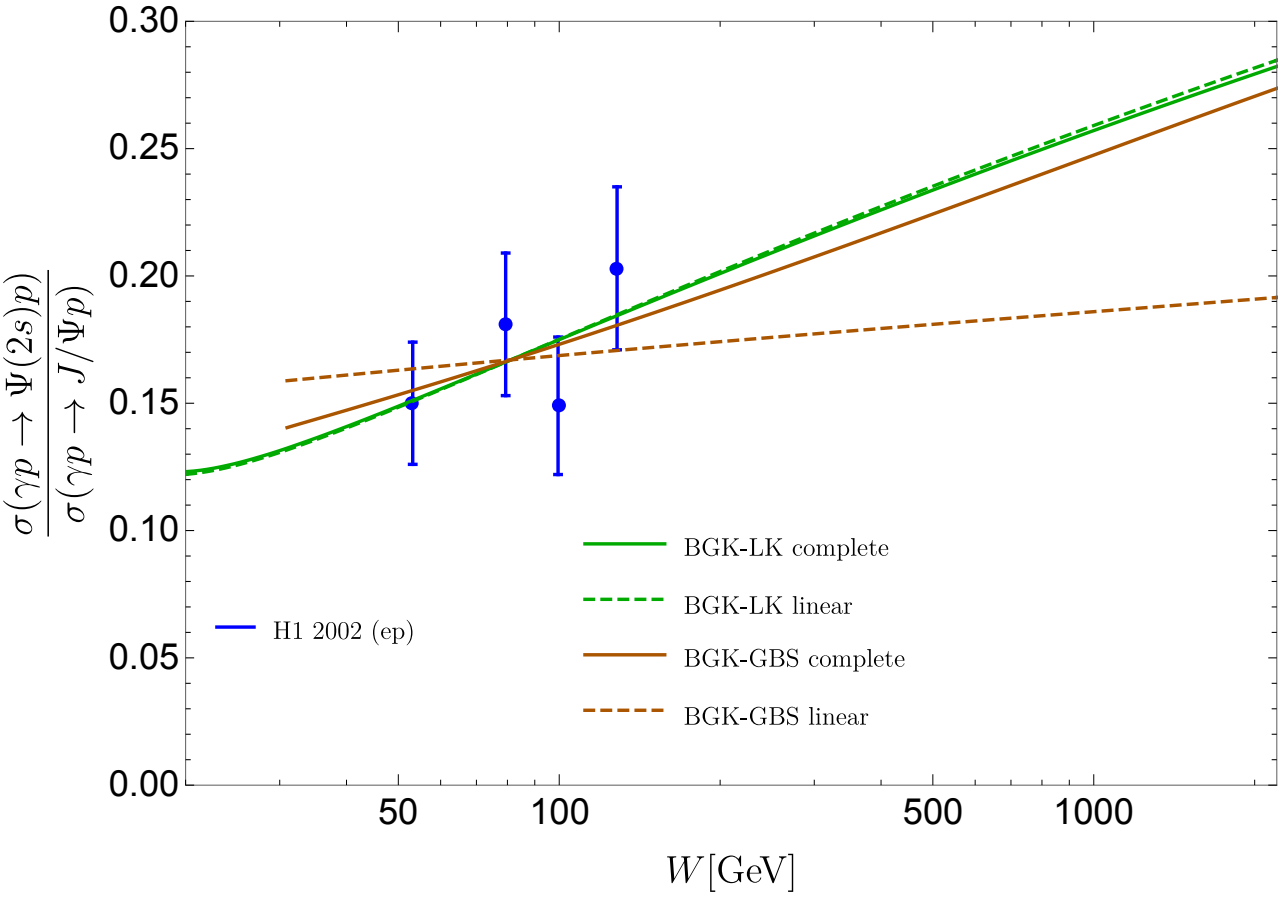


Figure 19: The energy dependence of the ratio of $\Psi(2s)$ and $J/\psi$ photo-production cross-section as provided by the BGK saturation model for gluon distribution considering two different fits: the LK and the GBS. (see [22] and [30]).

It is further displayed the photo-production data measured at HERA by H1 collaboration [7]. For the GBS fit, the linear NLO BFKL evolution predicts a ratio which is approximately constant with the energy of the photo-production cross-section, while the non-linear BK evolution predicts an increase with the energy of the cross-section ratio. As seen before, LK was not useful for differentiating linear NLO BFKL evolution and non-linear BK evolution. The fit was done for H1's highest precision data. Finally, The Buchmüller-Tye potential was chosen in order to give the numerical solution of the Schrödinger equation given by authors in [12] and [29].

## 5.2 Gaussian Wave-Functions

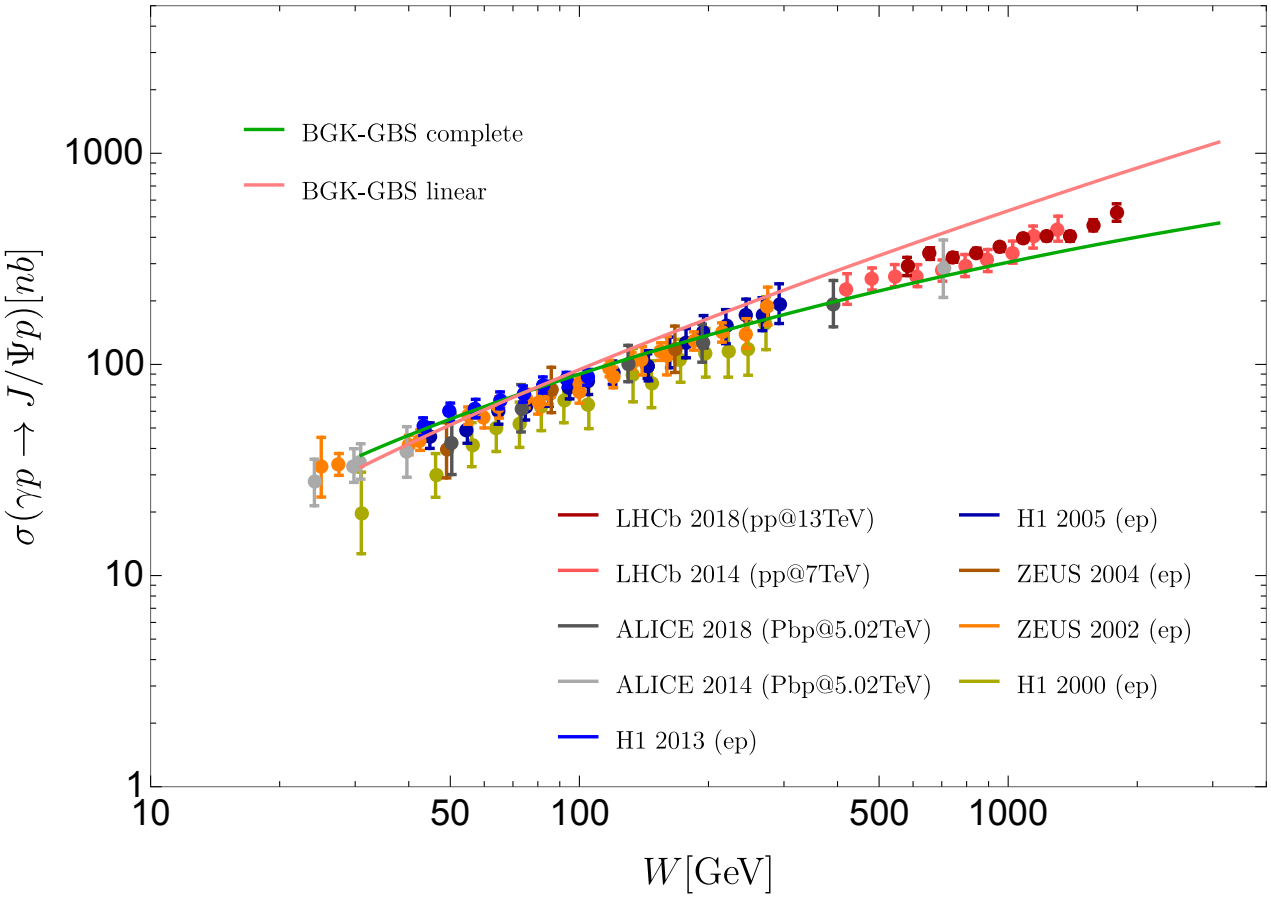


Figure 20: The energy dependence of the $J/\Psi$ photo-production cross-section process provided by the GBW and the BGK saturation models for gluon distribution implementing the GBS fit (see [22] ).

It is further displayed photo-production data measured at HERA by ZEUS ([14],[15]) and H1 ([7],[8],[9]) as well as LHC data obtained from ALICE ([4],[6]) and LHCb ($W^+$ solutions) ([2],[3]) collaborations. The fit was made to the highest precision data extracted from LHCb collaboration and the error bars displayed in figure 20 do not denote the complete uncertainty associated with these data points. As stated in the title, Gaussian functions were implemented to verify if the wave functions in some way affect the signs for the onset of non-linear QCD dynamics.

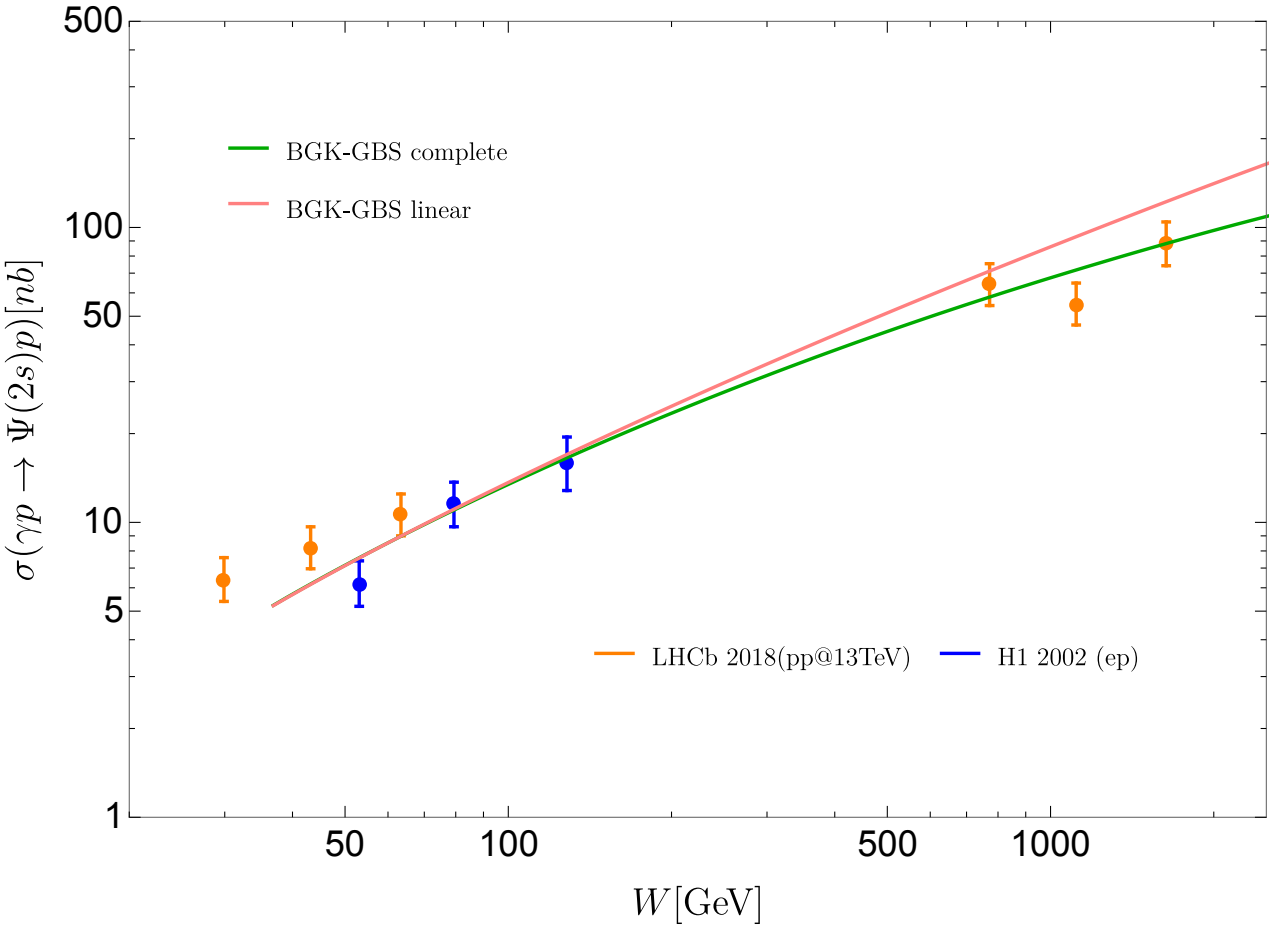


Figure 21: The energy dependence of the $\Psi(2s)$ photo-production cross-section process provided by the GBW and the BGK saturation models for gluon distribution implementing the GBS fit (see [22]).

We further display photo-production data measured at HERA by H1 ([7],[34]) as well as LHC data obtained from the LHCb collaboration ($W^+$ and $W^-$ solution) [3]. The BGK dipole model provides a rather excellent description of the energy dependence implementing the Gaussian wave functions and it's fitted to the highest precision data extracted from LHCb collaboration.

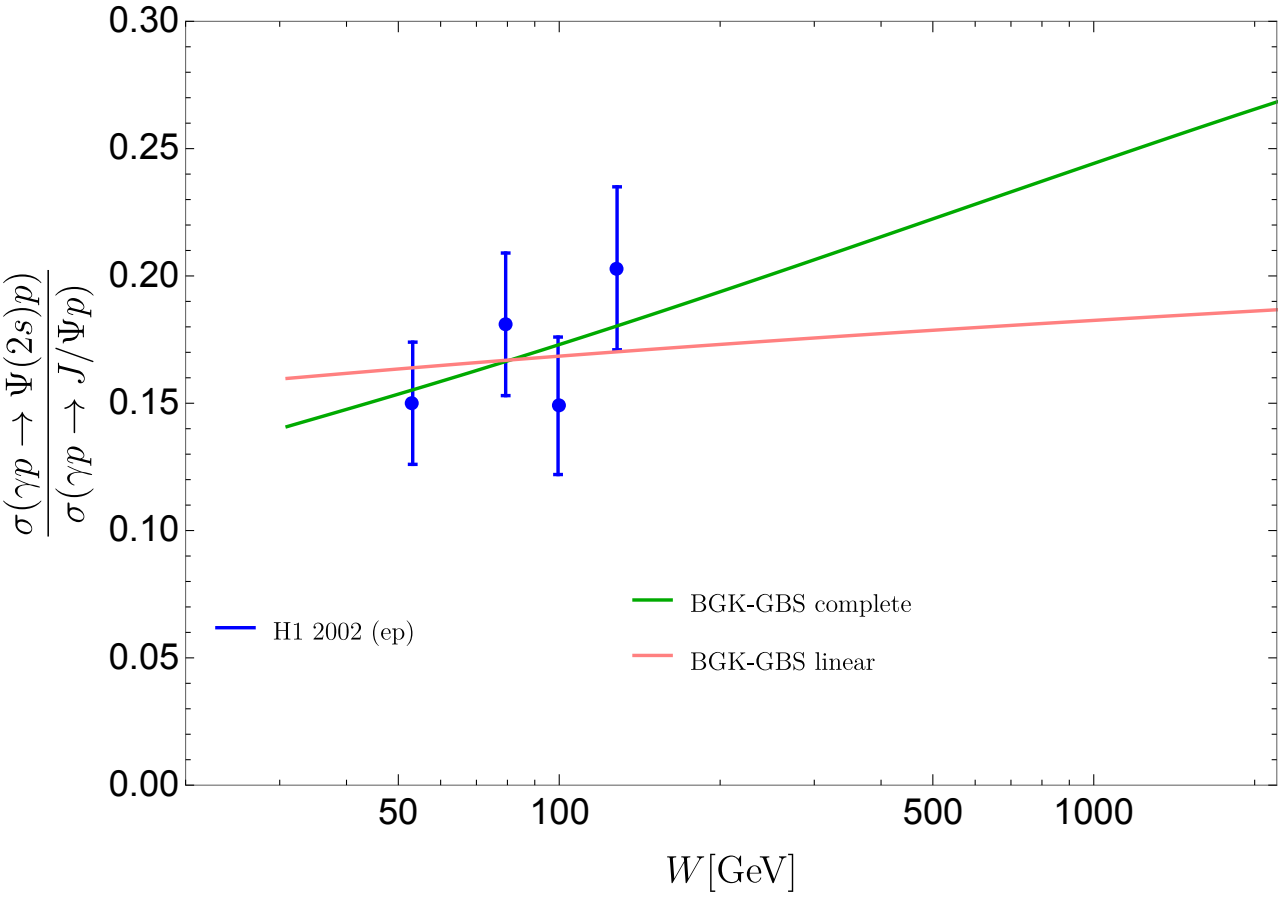


Figure 22: ratio

We further display photo-production data measured at HERA by H1 collaboration [7] and the most recent data extracted from ZEUS collaboration [39]. As in section one, for the GBS fit, the linear NLO BFKL evolution predicts a ratio which is approximately constant with the energy of the photo-production cross-section, while the non-linear BK evolution predicts an increase with the energy of the cross-section ratio.

## 5.3 Summarized results comparing two different saturation dipole models: the GBW and the BGK models implementing the GBS fit and a new parameter $k$.

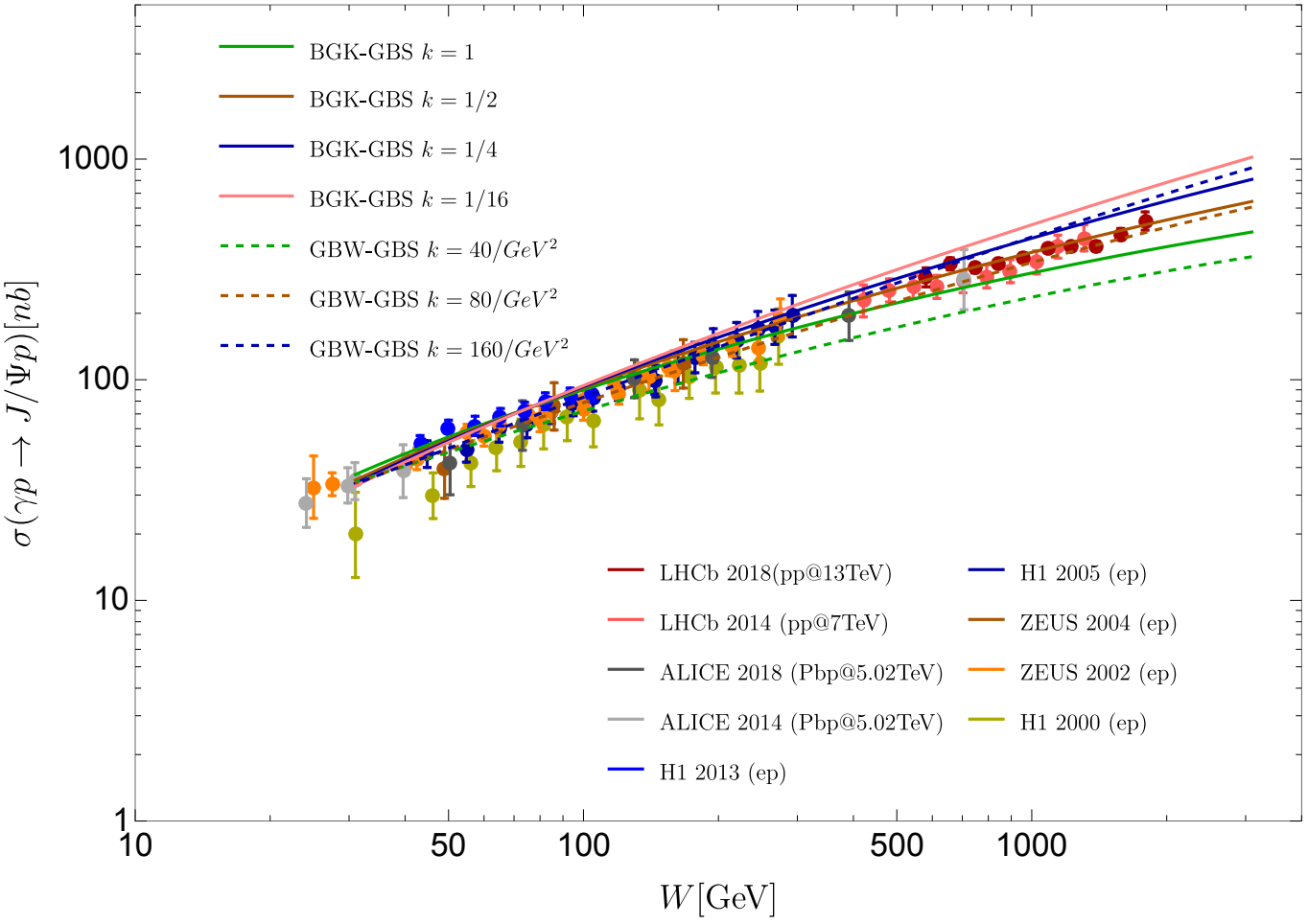


Figure 23: The energy dependence of the $J/\Psi$ photo-production cross-section process provided by the GBW and the BGK saturation models for gluon distribution implementing the GBS fit (see [22] ).

It is further displayed the photo-production data measured at HERA by ZEUS ([14],[15]) and H1 ([7],[8],[9]) as well as LHC data obtained from ALICE ([4],[6]) and LHCb ($W^+$ solutions) ([2],[3]) collaborations. Here there are two different dipole models implemented: the Golec-Biernat, Wuesthoff Model (GBW) and the Bartels, Golec-Biernat, Kowalski Model

(BGK). In both models, non-linear effects are simulated through exponentiating of the leading order QCD description, where the BGK model further includes DGLAP evolution into the description. On the other hand, the fit was made to the highest precision data extracted from LHCb collaboration and the error bars displayed in figure (23) do not denote the complete uncertainty associated with these data points. Lastly, the Gaussian wave functions were implemented for obtaining these results.

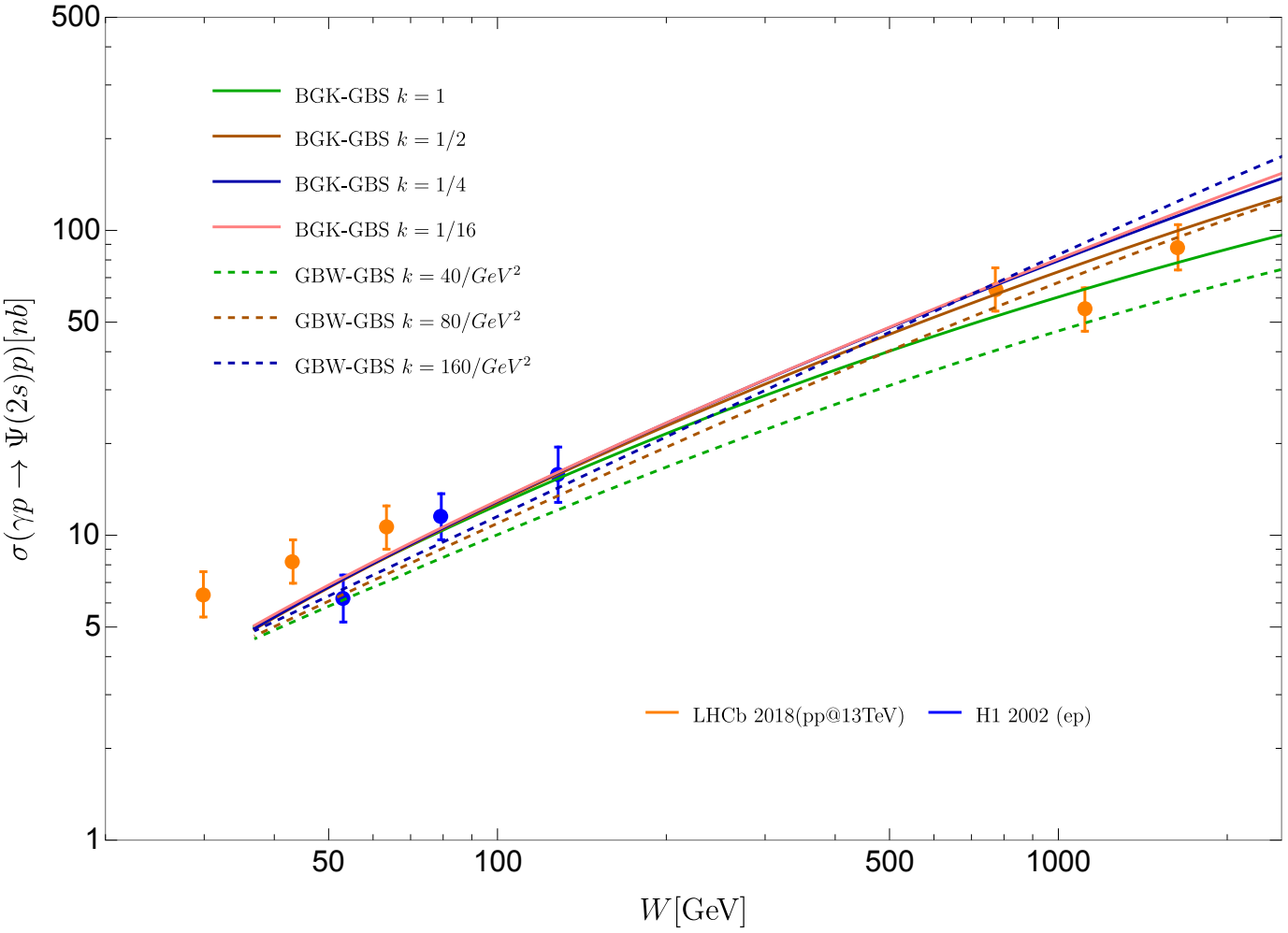


Figure 24: The energy dependence of the $\Psi(2s)$ photo-production cross-section process provided by the GBW and the BGK saturation models for gluon distribution implementing the GBS fit (see [22]).

We further display photo-production data measured at HERA by H1 ([7],[34]) as well

as LHC data obtained from the LHCb collaboration ($W^+$ and $W^-$ solution) [3]. Here two different dipole models were implemented: the Golec-Biernat, Wuesthoff Model (GBW) and the Bartels, Golec-Biernat, Kowalski Model (BGK). In both models, non-linear effects are simulated through exponentiating of the leading order QCD description, where the BGK model further includes DGLAP evolution into the description. On the other hand, the fit was made to the highest precision data extracted from the LHCb collaboration.

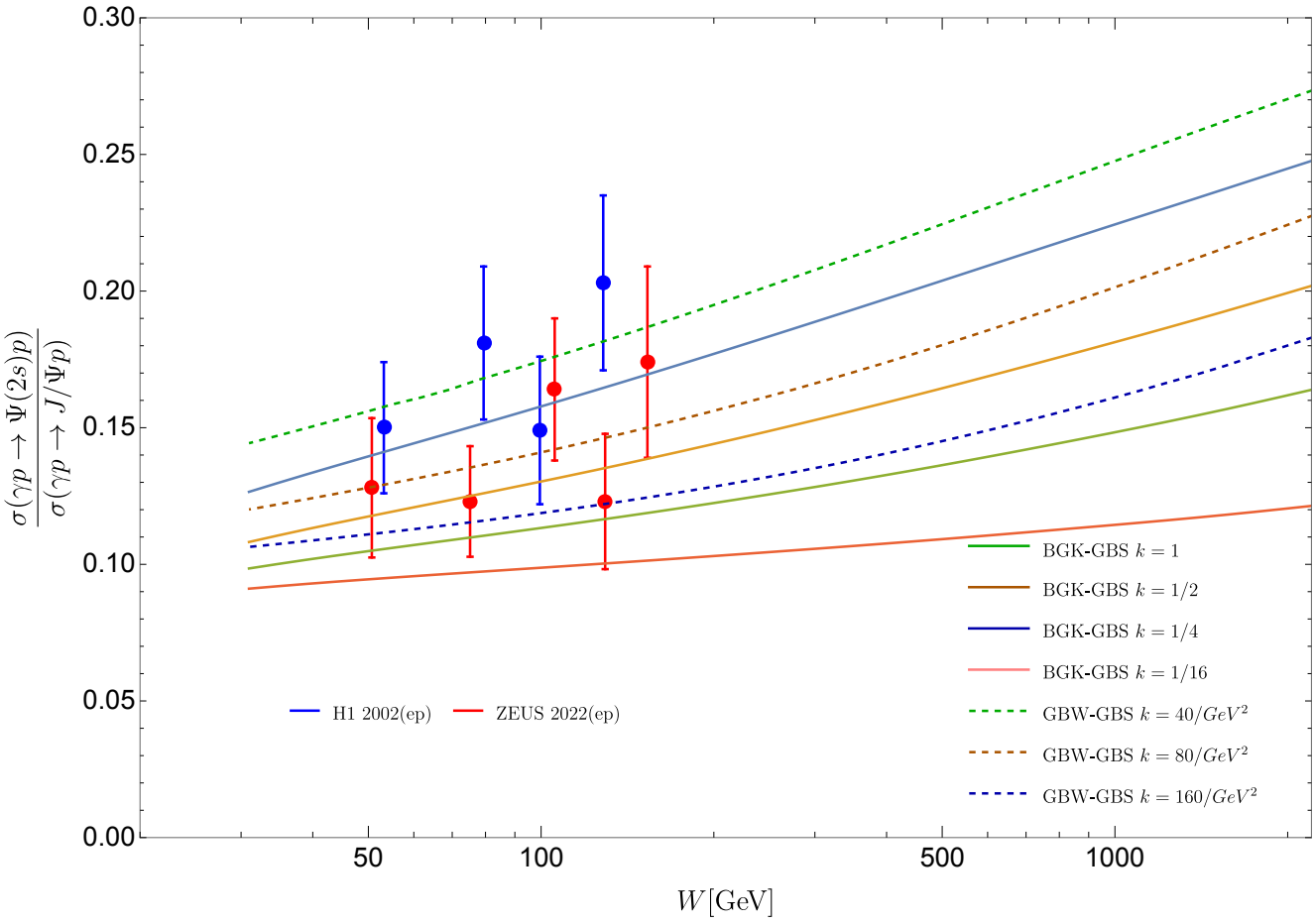


Figure 25: The energy dependence of the ratio of $\Psi(2s)$ and $J/\Psi$ photo-production cross-section process provided by the GBW and the BGK saturation models for gluon distribution implementing the GBS fit (see [22]).

We further display photo-production data measured at HERA by H1 collaboration [7] and the most recent data extracted from ZEUS collaboration [39]. Despite the fact for both dipole models, the parameter $k$ simulates non-linear effects through exponentiating of the

leading order QCD description, for the GBW model if this parameter $k$ is too big, the non-linear terms become relevant and for the BGK model, if this parameter k is too small, the non-linear terms become relevant. The linear NLO BFKL evolution predicts a ratio which is approximately constant with the energy of the photo-production cross-section, but when $k$ is big enough the non-linear BK evolution predicts an increase with the energy of the cross-section ratio for the GBW model. On the other hand, the linear NLO BFKL evolution predicts a ratio which is approximately constant with the energy of the photo-production cross-section, but when $k$ is small enough the non-linear BK evolution predicts an increase with the energy of the cross-section ratio for the BGK model. Finally, this fit was made with the newest and highest precision data extracted from the ZEUS collaboration.

# 6. Conclusions

It can be concluded that it seems most likely that non-linear effects start to become relevant at LHC, but their effects can be still absorbed into initial conditions of fits.
Secondly, it can be assured that the BGK model for gluon distribution does not depend on what wave function you implement, it still describes accurately the same phenomena.
Now, talking about the LK Fit, it can be affirmed that the difference between the linear and non-linear regimes for the BGK model is almost zero. The reason for that was that the tables for $\sigma_0$ the authors proportioned us for this study didn't have the correct parameters and hence, it couldn't be differentiated between linear and non-linear effects when the BGK model was implemented this fit.
It can also be concluded that we found a similar effect but in a smaller magnitude between the BFKL and BK evolution. The cross-section doesn't grow infinitely, even though you hypothetically put *infinite* energy in the system. This means, that the number of partons with a fraction of momentum $x$ inside the nuclei will not grow infinitely, but will eventually stabilize in a value.
It can be also affirmed that a constant ratio with the energy of $\Psi(2s)$ and $J/\Psi$ cross-section could hint at the absence of non-linear effects; also seen in [25], but it requires further anal-

ysis.

On the other hand, when both HERA and LHC data are compared, it is found that the differences between linear and non-linear implementations are relatively small at the level of photo-production cross-sections, in particular, if both theoretical and experimental uncertainties are taken into account.
It was also found that the ratio grows with energy in the presence of non-linear effects, while it remains approximately constant if non-linear effects are absent.
In particular for the GBW model if the parameter $k$ is too big, the non-linear terms become relevant; if it approaches zero, everything also becomes zero, and if it approaches one, it causes no hierarchy and the importance of terms is only determined by the saturation scale $Q_s^2(x)$. At last but not least, we can make the same analysis for the BGK saturation model; but instead of plugging an enormous value inside $k$, we plug a very minuscule value inside it and therefore we start to see that the non-linear terms also become relevant. If we fix the normalization, we see that $k$ is only reflected at the higher energies of the LHC. Finally, it can be affirmed that for the ratio, the curvature is changing with $k$.

# References

[1] LHC Machine. *JINST*, 3:S08001, 2008.

[2] R Aaij et al. Exclusive $J/\psi$ and $\psi$(2S) production in pp collisions at $\sqrt{s} = 7$ TeV. *J. Phys. G*, 40:045001, 2013.

[3] Roel Aaij et al. Central exclusive production of $J/\psi$ and $\psi(2S)$ mesons in $pp$ collisions at $\sqrt{s} = 13$ TeV. *JHEP*, 10:167, 2018.

[4] Betty Bezverkhny Abelev et al. Exclusive J/$\psi$ photoproduction off protons in ultra-peripheral p-Pb collisions at $\sqrt{s_{\rm NN}} = 5.02$ TeV. *Phys. Rev. Lett.*, 113(23):232504, 2014.

[5] A. Accardi et al. Electron Ion Collider: The Next QCD Frontier: Understanding the glue that binds us all. *Eur. Phys. J. A*, 52(9):268, 2016.

[6] Shreyasi Acharya et al. Energy dependence of exclusive J/$\psi$ photoproduction off protons in ultra-peripheral p–Pb collisions at $\sqrt{s_{\rm NN}}$ = 5.02 TeV. *Eur. Phys. J. C*, 79(5):402, 2019.

[7] C. Adloff et al. Diffractive photoproduction of psi(2S) mesons at HERA. *Phys. Lett. B*, 541:251–264, 2002.

[8] A. Aktas et al. Elastic J/psi production at HERA. *Eur. Phys. J. C*, 46:585–603, 2006.

[9] C. Alexa et al. Elastic and Proton-Dissociative Photoproduction of J/psi Mesons at HERA. *Eur. Phys. J. C*, 73(6):2466, 2013.

[10] Jonathan Allday. *Quarks, leptons and the big bang*. CRC Press, 2016.

[11] Niels Bohr. I. on the constitution of atoms and molecules. *The London, Edinburgh, and Dublin Philosophical Magazine and Journal of Science*, 26(151):1–25, 1913.

[12] Jan Cepila, Jan Nemchik, Michal Krelina, and Roman Pasechnik. Theoretical uncertainties in exclusive electroproduction of s-wave heavy quarkonia. *The European Physical Journal C*, 79(6):1–29, 2019.

[13] Jan Cepila, Jan Nemchik, Michal Krelina, and Roman Pasechnik. Theoretical uncertainties in exclusive electroproduction of S-wave heavy quarkonia. *Eur. Phys. J. C*, 79(6):495, 2019.

[14] S. Chekanov et al. Exclusive photoproduction of J / psi mesons at HERA. *Eur. Phys. J. C*, 24:345–360, 2002.

[15] S. Chekanov et al. Exclusive electroproduction of J/psi mesons at HERA. *Nucl. Phys. B*, 695:3–37, 2004.

[16] W Noel Cottingham and Derek A Greenwood. *An introduction to the standard model of particle physics*. Cambridge university press, 2007.

[17] R. Keith Ellis, W. James Stirling, and B. R. Webber. *QCD and collider physics*, volume 8. Cambridge University Press, 2 2011.

[18] Joël Feltesse. Introduction to deep inelastic scattering: past and present. In *Proceedings, 20th International Workshop on Deep-Inelastic Scattering and Related Subjects (DIS 2012)*, pages 3–12, 2012.

[19] RP Feynman, Murray Gell-Mann, and George Zweig. Group u (6)â u (6) generated by current components. *Physical Review Letters*, 13(22):678, 1964.

[20] Jean-Pierre Françoise, Gregory L Naber, and Sheung Tsun Tsou. *Encyclopedia of mathematical physics*, volume 2. Elsevier Amsterdam, 2006.

[21] Sheldon L Glashow, Jean Iliopoulos, and Luciano Maiani. Weak interactions with lepton-hadron symmetry. *Physical review D*, 2(7):1285, 1970.

[22] Krzysztof Golec-Biernat and Sebastian Sapeta. Saturation model of DIS : an update. *JHEP*, 03:102, 2018.

[23] Krzysztof J. Golec-Biernat and M. Wusthoff. Saturation effects in deep inelastic scattering at low Q**2 and its implications on diffraction. *Phys. Rev. D*, 59:014017, 1998.

[24] Thomas Heinze, Olof Hallonsten, and Steffi Heinecke. Turning the ship: The transformation of desy, 1993–2009. *Physics in Perspective*, 19(4):424–451, 2017.

[25] Martin Hentschinski and Emilio Padrón Molina. Exclusive $J/\Psi$ and $\Psi(2s)$ photoproduction as a probe of QCD low $x$ evolution equations. *Phys. Rev. D*, 103(7):074008, 2021.

[26] Henry W Kendall. Deep inelastic scattering: Experiments on the proton and the observation of scaling. *Reviews of Modern Physics*, 63(3):597, 1991.

[27] Yuri V Kovchegov and Eugene Levin. *Quantum chromodynamics at high energy*. Cambridge University Press, 2012.

[28] H Kowalski, L Motyka, and G Watt. Exclusive diffractive processes at hera within the dipole picture. *Physical Review D*, 74(7):074016, 2006.

[29] Michal Krelina, Jan Nemchik, Roman Pasechnik, and Jan Čepila. Spin rotation effects in diffractive electroproduction of heavy quarkonia. *The European Physical Journal C*, 79(2):1–15, 2019.

[30] Agnieszka Luszczak and Henri Kowalski. Dipole model analysis of highest precision HERA data, including very low $Q^2$'s. *Phys. Rev. D*, 95(1):014030, 2017.

[31] Ruprecht Machleidt. Nuclear forces. In *AIP Conference Proceedings*, volume 1541, pages 61–103. American Institute of Physics, 2013.

[32] Kenzo Nakamura. Review of particle physics. *Journal of Physics G: Nuclear and Particle Physics*, 37(7 A), 2010.

[33] F Nichitiu. An introduction to the vector mesons. In *Hadron Spectroscopy and the Confinement Problem*, pages 219–240. Springer, 1996.

[34] D. Schmidt. *Diffractive photoproduction of charmonium in the H1 detector at HERA*. PhD thesis, Hamburg U., 2001.

[35] Joseph John Thomson. Xl. cathode rays. *The London, Edinburgh, and Dublin Philosophical Magazine and Journal of Science*, 44(269):293–316, 1897.

[36] Joseph John Thomson. Xxiv. on the structure of the atom: an investigation of the stability and periods of oscillation of a number of corpuscles arranged at equal intervals around the circumference of a circle; with application of the results to the theory of atomic structure. *The London, Edinburgh, and Dublin Philosophical Magazine and Journal of Science*, 7(39):237–265, 1904.

[37] Eef Van Beveren and George Rupp. Scalar and axial-vector mesons. *The European Physical Journal A*, 31(4):468–473, 2007.

[38] Hideki Yukawa. On the interaction of elementary particles. i. *Proceedings of the Physico-Mathematical Society of Japan. 3rd Series*, 17:48–57, 1935.

[39] ZEUS Collaboration. Measurement of the cross-section ratio $\sigma_{\Psi(2s)}/\sigma_{J/\Psi(1S)}$ in exclusive photoproduction at hera, 2022.